Original Article

Dynamical behaviours and stability analysis of a generalized fractional model with a real case study

D. Baleanu [a,b,c], S. Arshad [d], A. Jajarmi [e,*], W. Shokat [d], F. Akhavan Ghassabzade [f], M. Wali [d]

[a] Department of Mathematics, Faculty of Arts and Sciences, Çankaya University, 06530 Ankara, Turkey
[b] Institute of Space Sciences, P.O.Box, MG-23, R 76900, Magurele-Bucharest, Romania
[c] Department of Medical Research, China Medical University Hospital, China Medical University, Taichung, Taiwan
[d] COMSATS University Islamabad, Lahore Campus, Lahore 54000, Pakistan
[e] Department of Electrical Engineering, University of Bojnord, P.O. Box, 94531-1339, Bojnord, Iran
[f] Department of Mathematics, Faculty of Sciences, University of Gonabad, Gonabad, Iran

HIGHLIGHTS

- A new and efficient fractional model is explored for the investigation of COVID-19 dynamics.
- The associated dynamical behaviors are discussed in terms of equilibrium points, invariant region, etc.
- To implement the proposed model numerically, an efficient approximation scheme is also employed.
- Simulation results are compared with a real case of COVID-19 pandemic in Italy.
- As a result, the new fractional model simulates the reality more precisely than the other classical frameworks.

GRAPHICAL ABSTRACT
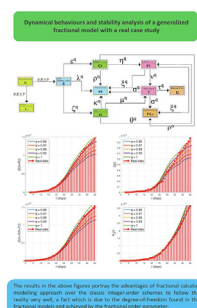
ARTICLE INFO

ABSTRACT

Introduction: Mathematical modelling is a rapidly expanding field that offers new and interesting opportunities for both mathematicians and biologists. Concerning COVID-19, this powerful tool may help humans to prevent the spread of this disease, which has affected the livelihood of all people badly.

Objectives: The main objective of this research is to explore an efficient mathematical model for the investigation of COVID-19 dynamics in a generalized fractional framework.

Methods: The new model in this paper is formulated in the Caputo sense, employs a nonlinear time-varying transmission rate, and consists of ten population classes including susceptible, infected, diagnosed, ailing, recognized, infected real, threatened, diagnosed recovered, healed, and extinct people. The existence of a unique solution is explored for the new model, and the associated dynamical behaviours are discussed in terms of equilibrium points, invariant region, local and global stability, and basic reproduction number. To implement the proposed model numerically, an efficient approximation scheme is employed by the combination of Laplace transform and a successive substitution approach; besides, the corresponding convergence analysis is also investigated.

Results: Numerical simulations are reported for various fractional orders, and simulation results are compared with a real case of COVID-19 pandemic in Italy. By using these comparisons between the simulated

---

and measured data, we find the best value of the fractional order with minimum absolute and relative errors. Also, the impact of different parameters on the spread of viral infection is analyzed and studied.
Conclusion: According to the comparative results with real data, we justify the use of fractional concepts in the mathematical modelling, for the new non-integer formalism simulates the reality more precisely than the classical framework.

Introduction

Coronavirus is an extreme faction of diseases that may originate the destruction of humanity. This virus has emerged as a horrible epidemic for human in the world from the earth's origin until now. The spread of coronavirus has affected the livelihood of all people badly, and a huge number of people have suffered from this virus so far. On December 2019, many unfamiliar probes of lung inflammation with cough, illness, tiredness, and labored breathing, as the main indication of this disease, appeared in Wuhan, China. The health jurisdiction of China as well as its central disease control (CDC) rapidly recognized the origin of these symptoms, a virus from the class of coronaviruses, and it was named as COVID-19 by the World Health Organization (WHO). Then for the recognition of this virus, several scientists and mathematicians have been doing a lot of researches [1–3]. In Italy, after the appearance of the first native case in a small town near Milan on February 21, 2020, many doubtful cases began to come out in the whole province, where 4,464,005 confirmed cases and 128,634 deaths from COVID-19 were certified since August 21, 2021. An alarming situation surrounded the whole area in which this infectious disease became endemic, so lockdown was initiated to control its upcoming disaster. Also, the public authority of Italy took various measures, including the implementation of sterile mindfulness and the isolation of infected patients. Additionally, all international flights were closed as well as educational institutions, trade centers, and picnic points. Meanwhile, clinical preliminaries and epidemiological observations were dispatched with the aim of securing the population.

Mathematical modelling is a rapidly expanding field that offers new and interesting opportunities for mathematicians, biologists, and other scientists [4–7]. Mathematical models provide an analytical framework to analyze and control different diseases [8]. Recently, mathematical formulations on the basis of nonlinear ordinary differential equations (ODEs) have been proposed for the quantitative analysis of COVID-19 pandemic. There are several generally utilized models including different strategies like *SIER* (susceptible, infectious, exposed, recovered), *SIRD* (susceptible, infected, recovered, dead), *SEIQV* (susceptible, exposed, infected, quarantine, vaccinated), and *SEIDARQ* (susceptible, exposed, infected, diagnosed, ailing, recovered, and quarantine), which were used to detect the transmission rate of COVID-19 from human to human [9]. As an example, the authors in [10] introduced an *SIDARTHE* model (susceptible, infected, diagnosed, ailing, recovered, threat, healed, extinct) model, consisting of eight states, and discussed its associated advantages and limitations.

Fractional calculus has been regarded as a strong mathematical tool for investigating aberrant processes found in different fields with notable memory and hereditary characteristics [11–13]. Over the past decades, a considerable number of valuable efforts have been done on the theoretical aspects of fractional calculus as well as its practical importance [14–16]. For instance, the authors in [17] examined a Van der Pol damping model by a fractional methodology. In [18], a fractional compartmental model was employed to investigate the dynamical behaviour of a drinking population. In [19], the numerical solution of fractional Lienard model was constructed by a reliable analytical scheme. In [20],

time–space fractional diffusion equations were investigated including fractional Sturm–Liouville operators for space and Caputo fractional derivatives in time. Another interesting study can also be found in [21] where a diffusion equation was considered in a time–space fractional framework. The advantages of fractional differential equations (FDEs) over the models of integer-order, such as those discussed in [22,23], motivate the researchers to investigate fractional-order compartmental models in order to gain a better grasp of complex phenomena [24–26]. To examine the emergence of various diseases, some non-integer order models have also been suggested; for instance, one can see the models for the spread of malaria [27], Zika virus [28], and dengue fever [29], all of which have epidemiologically been confirmed, mathematically been examined, experimentally been collaborated, and computationally been simulated.

Inspired by the aforementioned advantages of fractional mathematical modelling, this research explores the dynamics of COVID-19 pandemic by introducing a new system of FDEs. The main contributions of present study and the new developments obtained from this article are highlighted and emphasized as follows:

- The proposed model consists of ten population classes including susceptible, infected, diagnosed, ailing, recognized, infected real, threatened, diagnosed recovered, healed, and extinct people, collectively termed as $SIDARI_rTH_dHE$, and employs a nonlinear time-varying transmission rate.
- The existence of a unique solution is discussed for the new model, and the corresponding dynamical behaviours are investigated in terms of equilibrium points, invariant region, local and global stability, and basic reproduction number.
- An efficient numerical method is formulated by the combination of Laplace transform and a successive substitution strategy for the intention of numerical implementation, and a convergence analysis is given for the considered approximation scheme.
- To justify the use of fractional mathematical modelling, some comparisons are performed between the numerical results and a set of real clinical observations in Italy [30].
- Based on the above-mentioned comparative discussions, the best value of the fractional order is found with minimum absolute and relative errors. Besides, the impact of different parameters is studied on the spread of viral infection.

As a result, since the considered model has a flexible structure due to the existence of its fractional order parameter, it has the potential of extracting the hidden aspects of the real case study under investigation more accurately than the existing classical framework. Consequently, we believe that the fractional model, its solution method, and the associated mathematical discussions, presented in this paper, are new and comprise quite different information than their corresponding classical counterparts. Because of these advantages, we are of the opinion that the obtained results in this paper are noteworthy from both biological and mathematical viewpoints.

The remaining parts of this article is organized as follows. In the next section, we propose a mathematical model for the COVID-19

pandemic in the framework of fractional calculus. Then the dynamical behaviours regarding the new model are discussed. After that, we present a numerical method and discuss the biological significance of the results. Finally, some conclusions and future recommendations close the manuscript in the last section.

Preliminaries and new formulation

To understand the new model formulation, described in this section, first we define some basic definitions in the area of fractional calculus. Then we introduce the fractional model of $SIDARI_rTH_dHE$ for the COVID-19 pandemic.

Definitions

Definition 1. For a function $f : [0, T] \rightarrow \mathbb{R}, q \in (n - 1, n)$, and $n \in \mathbb{N}$, the Riemann–Liouville fractional integral of order q is defined by [31]

$$\mathscr{I}_t^q f(t) = \frac{1}{\Gamma(q)} \int_0^t (t - u)^{q-1} f(u) du, \quad t \in [0, T]. \tag{1}$$

Definition 2. For a function $f : [0, T] \rightarrow \mathbb{R}, q \in (n - 1, n)$, and $n \in \mathbb{N}$, the Caputo fractional derivative of order q is given as [31]

$$\mathscr{D}_t^q f(t) = \frac{1}{\Gamma(n - q)} \int_0^t (t - u)^{n-q-1} f^{(n)}(u) du, \quad t \in [0, T]. \tag{2}$$

Besides, the Laplace transform of Caputo fractional derivative (2) is expressed by [31]

$$\mathscr{L}\left[\mathscr{D}_t^q f(t) \right] = s^q \mathscr{L}[f(t)] - \sum_{k=0}^{n-1} s^{q-k-1} f^{(k)}(0), \quad n - 1 < q < n, \ n$$
$$\in \mathbb{N}. \tag{3}$$

Also, we can rewrite the Eq. (3) more simply as

$$\mathscr{L}\left[\mathscr{D}_t^q f(t) \right] = \frac{s^n \mathscr{L}[f(t)] - s^{n-1} f(0) - s^{n-2} f\prime(0) - \ldots - f^{(n-1)}(0)}{s^{n-q}}. \tag{4}$$

Generalized fractional model

Various studies in life sciences, physics, engineering, and elsewhere have shown that fractional-order modelling could provide better agreement between simulated and measured data than its

integer-order counterpart (see, for example, [32] and the references therein). This important feature justifies the use of fractional-order models for the dynamical systems under consideration in different studies. In our case, it is worth mentioning that the original integer-order model with eight state variables was introduced and analyzed in [10], while a ten-state model was used in the corresponding programming codes in [10]. Here, we consider the original ten-state model in which we replace the integer-order derivatives with fractional-order ones. Also, according to the discussion in [33], we replace the value of each parameter in the system model by taking its power to the order of derivative (q) in order to achieve dimensional matching between the left and the right sides of the resultant fractional equations. As a result, we introduce the fractional-order model of $SIDARI_rTH_dHE$ with $0 < q < 1$ as follows

$$\mathscr{D}_t^q S(t) = -(\alpha^q I(t) + \beta^q D(t) + \gamma^q A(t) + \delta^q R(t)) S(t),$$
$$\mathscr{D}_t^q I(t) = -(\epsilon^q + \zeta^q + \lambda^q) I(t) + (\alpha^q I(t) + \beta^q D(t) + \gamma^q A(t) + \delta^q R(t)) S(t),$$
$$\mathscr{D}_t^q D(t) = -(\eta^q + \rho^q) D(t) + \epsilon^q I(t),$$
$$\mathscr{D}_t^q A(t) = -(\theta^q + \mu^q + \kappa^q) A(t) + \zeta^q I(t),$$
$$\mathscr{D}_t^q R(t) = -(\nu^q + \xi^q) R(t) + \eta^q D(t) + \theta^q A(t),$$
$$\mathscr{D}_t^q I_r(t) = (\alpha^q I(t) + \beta^q D(t) + \gamma^q A(t) + \delta^q R(t)) S(t),$$
$$\mathscr{D}_t^q T(t) = -(\sigma^q + \tau^q) T(t) + \mu^q A(t) + \nu^q R(t),$$
$$\mathscr{D}_t^q H_d(t) = \rho^q D(t) + \xi^q R(t) + \sigma^q T(t),$$
$$\mathscr{D}_t^q H(t) = \lambda^q I(t) + \rho^q D(t) + \kappa^q A(t) + \xi^q R(t) + \sigma^q T(t),$$
$$\mathscr{D}_t^q E(t) = \tau^q T(t).$$
$$\tag{5}$$

where the state variables are described by:

– Compartment of susceptible people is denoted by $S(t)$.
– Compartment of infected (asymptomatic infected, but undetected) individuals is symbolized by $I(t)$.
– Compartment of diagnosed (asymptomatic infected and detected) persons is displayed by $D(t)$.
– Compartment of ailing (symptomatic infected, but undetected) population is depicted by $A(t)$.
– $R(t)$ is the compartment of recognized (symptomatic infected and detected) persons.
– Compartment of actual currently infected people is portrayed by $I_r(t)$.
– $T(t)$ is the compartment of threatened (infected with life-threatening symptoms and detected) population.
– H_d is the compartment of diagnosed and recovered individuals.
– Healed compartment is presented by $H(t)$.
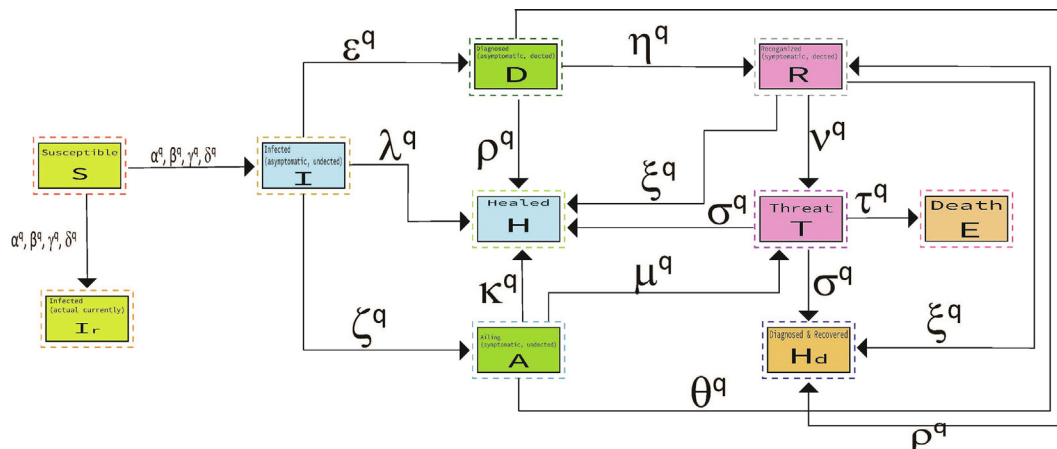– $E(t)$ is the extinct compartment population.

Fig. 1. Flowchart of the $SIDARI_rTH_dHE$ model.

The descriptions of the other parameters are also given as:

- $\alpha^q, \beta^q, \gamma^q$, and δ^q denote the transmission rates from the susceptible stage into the infected, diagnosed, ailing, and recognized phases, respectively.
- ϵ^q and θ^q are the rates of detection relative to asymptomatic and symptomatic cases, respectively.
- ζ^q and η^q denote the rates of awareness and non-awareness from being infected, respectively.
- μ^q and ν^q are the rates at which undetected and detected states go to the threaten stage, respectively.
- τ^q is the death rate in which the threaten people go to the extinct population.
- $\lambda^q, \kappa^q, \xi^q$, and σ^q are the rates of recovery from different five stages, respectively.

The flowchart of the $SIDARI_rTH_dHE$ model is shown in Fig. 1.

Existence and uniqueness

This section presents a qualitative existence and uniqueness analysis for the suggested system (5). The relevant theory in this part makes sure that the considered model for every biological dynamics is properly stated. To this aim, researchers used a variety of methods, one of which is the Banach contraction theorem. Here, we employ this approach to show the existence of a unique solution for the model under consideration. For this purpose, we rewrite the system (5) in a compact form as below

$$\begin{cases} \mathscr{D}_t^q F(t) = \Theta(F(t)), & t \in [0, T], \\ F(0) = F_0, \end{cases} \tag{6}$$

where $F(t) = (S(t), I(t), D(t), A(t), R(t), I_r(t), T(t), H_d(t), H(t), E(t))$,

$$\Theta(F(t)) = \begin{bmatrix} -(\alpha^q I(t) + \beta^q D(t) + \gamma^q A(t) + \delta^q R(t))S(t) \\ -(\epsilon^q + \zeta^q + \lambda^q)I(t) + (\alpha^q I(t) + \beta^q D(t) + \gamma^q A(t) + \delta^q R(t))S(t) \\ -(\eta^q + \rho^q)D(t) + \epsilon^q I(t) \\ -(\theta^q + \mu^q + \kappa^q)A(t) + \zeta^q I(t) \\ -(\nu^q + \xi^q)R(t) + \eta^q D(t) + \theta^q A(t) \\ (\alpha^q I(t) + \beta^q D(t) + \gamma^q A(t) + \delta^q R(t))S(t) \\ -(\sigma^q + \tau^q)T(t) + \mu^q A(t) + \nu^q R(t) \\ \rho^q D(t) + \xi^q R(t) + \sigma^q T(t) \\ \lambda^q I(t) + \rho^q D(t) + \kappa^q A(t) + \xi^q R(t) + \sigma^q T(t) \\ \tau^q T(t) \end{bmatrix}, \tag{7}$$

and F_0 denotes the initial state vector. Applying the Riemann–Liouville integral (Definition 1) to the both sides of the Eq. (6), we can express

$$F(t) = F_0 + \frac{1}{\Gamma(q)} \int_0^t (t-u)^{q-1} \Theta(F(u)) du, \quad t \in [0, T]. \tag{8}$$

Let $\mathbb{X} = ([0, T], \| \cdot \|)$ be a Banach space with the norm

$$\|F(t)\| = \max_{t \in [0,T]} [|S(t)| + |I(t)| + |D(t)| + |A(t)| + |R(t)| + |I_r(t)| + |T(t)| + |H_d(t)| + |H(t)| + |E(t)|]. \tag{9}$$

We also assume that the following presumptions are true for any additional implications of the considered problem:

- (P_1): The constants K_* and M_* exist such that

$$\|\Theta(F(t))\| \leqslant K_* \|F(t)\|^l + M_*. \tag{10}$$

- (P_2): For each $F(t)$ and $\overline{F}(t)$, there exists a constant L_* such that

$$\|\Theta(F(t)) - \Theta(\overline{F}(t))\| \leqslant L_* \|F(t) - \overline{F}(t)\|. \tag{11}$$

Further, the operator $\Pi : \mathbb{X} \to \mathbb{X}$ is defined by

$$\Pi F(t) = F_0 + \frac{1}{\Gamma(q)} \int_0^t (t-u)^{q-1} \Theta(F(u)) du. \tag{12}$$

Theorem 1. The problem (6) has at least one fixed point according to the assumptions (P_1) and (P_2). This implies that there is at least one solution to the problem under consideration.

Proof. Using the Schaefer's fixed point theorem, we will proceed in four steps as follows:

Step 1: In order to show that Π is continuous, we consider that $F_n(t)$ is a sequence of continuous functions for $n = 1, 2, \ldots$; thus, $\Theta(F_n(t))$ is also continuous. Let $F_n(t), F(t) \in \mathbb{X}$ such that $F_n(t) \to F(t)$; then we must have $\Pi F_n(t) \to \Pi F(t)$. To show this, consider

$$\begin{aligned} \|\Pi F_n(t) - \Pi F(t)\| &= \left\| \frac{1}{\Gamma(q)} \int_0^t (t-u)^{q-1} \Theta(F_n(u)) du - \frac{1}{\Gamma(q)} \int_0^t (t-u)^{q-1} \Theta(F(u)) du \right\| \\ &\leqslant \max_{t \in [0,T]} \int_0^t \left| \frac{(t-u)^{q-1}}{\Gamma(q)} \right| \|\Theta(F_n(u)) - \Theta(F(u))\| du \\ &\leqslant \frac{T^q L_*}{\Gamma(q+1)} \|F_n(t) - F(t)\| \to 0 \quad as \quad n \to \infty. \end{aligned} \tag{13}$$

Since $F(t)$ is continuous, as a result, Π is also continuous, and therefore, $\Pi F_n(t) \to \Pi F(t)$.

Step 2: Now, we show that the map Π is bounded. For this purpose, let $F(t) \in \mathbb{X}$; then the following growth condition is satisfied by Π

$$\begin{aligned} \|\Pi F(t)\| &= \left\| F_0 + \frac{1}{\Gamma(q)} \int_0^t (t-u)^{q-1} \Theta(F(u)) du \right\| \\ &\leqslant \|F_0\| + \max_{t \in [0,T]} \frac{1}{\Gamma(q)} \int_0^t \left| (t-u)^{q-1} \right| \|\Theta(F(u))\| du \\ &\leqslant \|F_0\| + \frac{T^q}{\Gamma(q+1)} \left(K_* \|F(t)\|^l + M_* \right). \end{aligned} \tag{14}$$

To show that $\Pi(\mathscr{S})$ is bounded for a bounded subset $\mathscr{S}$ of $\mathbb{X}$, let for any $F(t) \in \mathscr{S}$, since $\mathscr{S}$ is bounded, there exists a $P_* \geqslant 0$ such that

$$\|F(t)\| \leqslant P_*, \quad \forall F(t) \in \mathscr{S}. \tag{15}$$

Hence, using the growth condition given above, for any $F(t) \in \mathscr{S}$ we have

$$\begin{aligned} \|\Pi F(t)\| &\leqslant \|F_0\| + \frac{T^q}{\Gamma(q+1)} \left(K_* \|F(t)\|^l + M_* \right) \\ &\leqslant \|F_0\| + \frac{T^q}{\Gamma(q+1)} \left(K_* P_*^l + M_* \right). \end{aligned} \tag{16}$$

Therefore, $\Pi(\mathscr{S})$ is bounded.

Step 3: Let $t_1, t_2 \in [0, T]$ with $t_1 \geqslant t_2$; then

$$\begin{aligned} \|\Pi F(t_1) - \Pi F(t_2)\| &= \left\| \frac{1}{\Gamma(q)} \int_0^t (t_1 - u)^{q-1} \Theta(F(u)) du - \frac{1}{\Gamma(q)} \int_0^t (t_2 - u)^{q-1} \Theta(F(u)) du \right\| \\ &\leqslant \max_{t \in [0,T]} \frac{1}{\Gamma(q)} \int_0^t \left| (t_1 - u)^{q-1} - (t_2 - u)^{q-1} \right| \|\Theta(F(u))\| du \\ &\leqslant \frac{T^q}{\Gamma(q+1)} \left(K_* \|F(t)\|^l + M_* \right) (t_1 - t_2). \end{aligned} \tag{17}$$

Therefore, through Arzelà-Ascoli theorem, $\Pi(\mathscr{S})$ is relatively compact.

Step 4: In this step, we show that the set $\mathbf{H} = \{F(t) \in \mathbb{X} : F(t) = b\Pi F(t), b \in (0,1)\}$, is bounded. For this purpose, let $F(t) \in \mathbf{H}$; then for each $t \in [0,T]$ we have

$$\|F(t)\| = b\|\Pi F(t)\| \leqslant b\left[\|F_0\| + \frac{T^q}{\Gamma(q+1)}\left(K_*\|F(t)\|^l + M_*\right)\right]. \quad (18)$$

Therefore, the set $\mathbf{H}$ is shown to be bounded using the Schaefer's fixed point theorem. As a result, Π has at least one fixed point, and hence, there is at least one solution to our considered problem.

Remark 1. The conclusion of the above theorem holds true even if the assumption (P_1) is formulated with $q = 1$ when $\frac{T^q K_*}{\Gamma(q+1)} < 1$.

Theorem 2. The problem (6) has a unique solution if $\frac{T^q K_*}{\Gamma(q+1)} < 1$.

Proof. In order to use the Banach contraction theorem, let $F(t), \overline{F}(t) \in \mathbb{X}$; then

$$\begin{aligned}\|\Pi F(t) - \Pi\overline{F}(t)\| &\leqslant \max_{t \in [0,T]}\frac{1}{\Gamma(q)}\int_0^t\left|(t-u)^{q-1}\right|\left\|\Theta(F(u)) - \Theta(\overline{F}(u))\right\|du \\ &\leqslant \frac{T^q L_*}{\Gamma(q+1)}\|F(t) - \overline{F}(t)\|.\end{aligned}$$
$$(19)$$

Thus, Π has a unique fixed point, and hence, the considered problem (6) has a unique solution.

Dynamical behaviours

Equilibrium points

Equilibria refer to the states in which all working forces are cancelled out, resulting in a structure that is smooth, balanced, or unchanged. Additionally, the equilibrium point is a constant solution to a differential equation. Concerning the $SIDARI_rTH_dHE$ model (5), three equilibrium points exist as

$$\begin{aligned}&(S^*, 0, 0, 0, 0, 0, 0, 0, H^*, E^*),\\ &(S^{**}, 0, 0, 0, 0, 0, 0, H_d^{**}, H^{**}, E^{**}),\\ &(S^{***}, I^{***}, D^{***}, A^{***}, R^{***}, I_r^{***}, 0, H_d^{***}, H^{***}, E^{***}),\end{aligned} \quad (20)$$

and are described by the disease-free equilibrium (DFE), the diagnosed DFE, and the endemic steady-state, respectively.

The $SIDARI_rTH_dHE$ model (5) is a bilinear system with ten state variables; also, it is positive, which means that all its states are non-negative for $t \geqslant 0$ if they are initialized by non-negative values at $t = 0$. More to the point, let $N(t)$ denote the total population defined by

$$\begin{aligned}N(t) = &S(t) + I(t) + D(t) + A(t) + R(t) + I_r(t) + T(t) + H_d \\ &+ H(t) + E(t).\end{aligned} \quad (21)$$

Then we can write

$$\begin{aligned}\mathscr{D}_t^q N(t) = &\mathscr{D}_t^q S(t) + \mathscr{D}_t^q I(t) + \mathscr{D}_t^q D(t) + \mathscr{D}_t^q A(t) + \mathscr{D}_t^q R(t) \\ &+ \mathscr{D}_t^q I_r(t) + \mathscr{D}_t^q T(t) + \mathscr{D}_t^q H_d(t) + \mathscr{D}_t^q H(t) + \mathscr{D}_t^q E(t) \\ = &0,\end{aligned} \quad (22)$$

since the model (5) is compartmental and exhibits the mass conversation property. As a consequence, since each state variable is a fraction of the total population, and as the total population is constant, we can suppose that $N(t) = 1$, in which 1 denotes the entire population including the extinct people. Additionally, if the sum of all initial conditions is equal to 1, then the system (5) converges

to the DFE with $S^*, H^*, E^* \geqslant 0$ and $S^* + H^* + E^* = 1$. In this condition when only the populations S, H, and E remain, we can say, from a biological point of view, that the outbreak phenomenon stops. Thus, here we discuss the DFE with $S^* + H^* + E^* = 1$. To do so, we partition the system (5) into three subsystems in order to better explain its dynamical behaviours:

- The first subsystem includes susceptible population S.
- The second subsystem contains the infected populations $[IDARI_rTH_d]$, which are non-zero only during the transient.
- The third subsystem includes the healed and the extinct populations H and E, respectively.

Here, it is worth mentioning that when $H_d + T + I_r + R + A + D + I = 0$, then the state variables S, H, E are at their steady-states S^*, H^*, E^*, respectively. In addition, $S(t), H(t), E(t)$ converge to S^*, H^*, E^* iff $H_d(t), T(t), I_r(t), R(t), A(t), D(t), I(t)$ converge to zero. In the following, we recast the overall system (5) in a feedback structure in which the subsystem $IDARI_rTH_d$ would be a positive linear system subject to a feedback signal U. For this purpose, defining $Y(t) = [I(t) \quad D(t) \quad A(t) \quad R(t) \quad I_r(t) \quad T(t) \quad H_d(t)]^T$, we can write the subsystem $IDARI_rTH_d$ as follows

$$\mathscr{D}_t^q Y(t) = \begin{bmatrix} -\omega_1 & 0 & 0 & 0 & 0 & 0 & 0 \\ \epsilon & -\omega_2 & 0 & 0 & 0 & 0 & 0 \\ \zeta^q & 0 & -\omega_3 & 0 & 0 & 0 & 0 \\ 0 & \eta^q & \theta^q & -\omega_4 & 0 & 0 & 0 \\ 0 & 0 & 0 & 0 & 0 & 0 & 0 \\ 0 & 0 & \mu^q & \nu^q & 0 & -\omega_5 & 0 \\ 0 & \rho & 0 & \xi & 0 & \sigma & 0 \end{bmatrix} Y(t) + \begin{bmatrix} 1 \\ 0 \\ 0 \\ 0 \\ 0 \\ 0 \\ 0 \end{bmatrix} U(t), \quad (23)$$

$$\begin{aligned}Z_s(t) &= \begin{bmatrix} \alpha^q & \beta^q & \gamma^q & \delta^q & 0 & 0 & 0 \end{bmatrix} Y(t),\\ Z_H(t) &= \begin{bmatrix} \lambda^q & \rho^q & \kappa^q & \xi^q & 0 & \sigma^q & 0 \end{bmatrix} Y(t),\\ Z_E(t) &= \begin{bmatrix} 0 & 0 & 0 & 0 & 0 & \tau^q & 0 \end{bmatrix} Y(t),\end{aligned} \quad (24)$$

where $\omega_1 = \epsilon^q + \zeta^q + \lambda^q, \omega_2 = \eta^q + \rho, \omega_3 = \theta^q + \mu^q + \kappa, \omega_4 = \nu^q + \xi, \omega_5 = \sigma + \tau^q$, and $U(t) = S(t)Z_s(t)$. Also, the leftover variables fulfill the expressions

$$\begin{aligned}\mathscr{D}_t^q S(t) &= -S(t)Z_s(t), &(27)\\ \mathscr{D}_t^q H(t) &= Z_H(t), &(28)\\ \mathscr{D}_t^q E(t) &= Z_E(t). &(29)\end{aligned}$$

Now, we can continue with the parametric study of local stability based on the asymptotic feedback gain S^*, for the time-varying feedback coefficient $S(t)$ finally tends to the constant gain S^*.

Local stability

Theorem 3. The subsystem $IDARI_rTH_d$ with the susceptible population S^* is asymptotically stable *iff*

$$S^* < \overline{S}^*, \quad (30)$$

where

$$\overline{S}^* = \frac{\omega_1\omega_2\omega_3\omega_4}{\alpha^q\omega_2\omega_3\omega_4 + \beta^q\epsilon^q\omega_3\omega_4 + \gamma^q\zeta^q\omega_2\omega_4 + \delta^q(\eta^q\epsilon^q\omega_3 + \zeta^q\theta^q\omega_2)}. \quad (31)$$

Proof. Concerning the overall system (5), the Jacobian matrix J around the DFE is computed as

$$
J = \begin{bmatrix}
0 & -\alpha^q S^* & -\beta^q S^* & -\gamma^q S^* & -\sigma S^* & 0 & 0 & 0 & 0 & 0 \\
0 & \alpha^q S^* - \omega_1 & \beta^q S^* & \gamma^q S^* & \delta^q S^* & 0 & 0 & 0 & 0 & 0 \\
0 & \epsilon^q & -\omega_2 & 0 & 0 & 0 & 0 & 0 & 0 & 0 \\
0 & \zeta^q & 0 & -\omega_3 & 0 & 0 & 0 & 0 & 0 & 0 \\
0 & 0 & \eta^q & \theta^q & -\omega_4 & 0 & 0 & 0 & 0 & 0 \\
0 & \alpha^q S^* & \beta^q S^* & \gamma^q S^* & \delta^q S^* & 0 & 0 & 0 & 0 & 0 \\
0 & 0 & 0 & \mu^q & v^q & 0 & -\omega_5 & 0 & 0 & 0 \\
0 & 0 & \rho & 0 & \xi & 0 & \sigma & 0 & 0 & 0 \\
0 & \lambda^q & \rho & \kappa & \xi & 0 & \sigma & 0 & 0 & 0 \\
0 & 0 & 0 & 0 & 0 & 0 & \tau^q & 0 & 0 & 0
\end{bmatrix}.
\tag{32}
$$

Thus, one can obtain

$$
det(J - mI) = \begin{vmatrix}
-m & -\alpha^q S^* & -\beta^q S^* & -\gamma^q S^* & -\delta^q S^* & 0 & 0 & 0 & 0 & 0 \\
0 & \alpha^q S^* - \omega_1 - m & \beta^q S^* & \gamma^q S^* & \delta^q S^* & 0 & 0 & 0 & 0 & 0 \\
0 & \epsilon^q & -\omega_2 - m & 0 & 0 & 0 & 0 & 0 & 0 & 0 \\
0 & \zeta^q & 0 & -\omega_3 - m & 0 & 0 & 0 & 0 & 0 & 0 \\
0 & 0 & \eta^q & \theta^q & -\omega_4 - m & 0 & 0 & 0 & 0 & 0 \\
0 & \alpha^q S^* & \beta^q S^* & \gamma^q S^* & \delta^q S^* & -m & 0 & 0 & 0 & 0 \\
0 & 0 & 0 & \mu^q & v^q & 0 & -\omega_5 - m & 0 & 0 & 0 \\
0 & 0 & \rho & 0 & \xi & 0 & \sigma & -m & 0 & 0 \\
0 & \lambda^q & \rho & \kappa & \xi & 0 & \sigma & 0 & -m & 0 \\
0 & 0 & 0 & 0 & 0 & 0 & \tau^q & 0 & 0 & -m
\end{vmatrix}.
\tag{33}
$$

Some algebraic manipulations using the above determinant show that the matrix J has five null eigenvalues, and the other five eigenvalues are obtained from the characteristic polynomial equation

$$
P(m) = D(m) - S^* N(m) = 0,
\tag{34}
$$

where

$$
D(m) = (\omega_1 + m)(\omega_2 + m)(\omega_3 + m)(\omega_4 + m)(\omega_5 + m),
\tag{35}
$$

and

$$
N(m) = (\omega_5 + m)(\alpha^q((\omega_2 + m)(\omega_3 + m)(\omega_4 + m))(\beta^q \epsilon^q)(\omega_3 + m)(\omega_4 + m)
$$
$$
+ \delta^q(\eta^q \epsilon^q(\omega_3 + m) + \theta^q \xi(\omega_2 + m)) + \gamma^q \xi(\omega_2 + m)(\omega_4 + m)).
\tag{36}
$$

In the system (23)–(26), $G(s) = \frac{N(s)}{D(s)}$ is the transfer function from U to Z_s. Also, the static gain $G(0) = \frac{N(0)}{D(0)}$ is the H_∞ norm of $G(s)$ since the system (23) is positive. Eventually, according to the standard root-locus analysis for positive systems, the polynomial in (34) is Hurwitz *iff* the required condition (30), in which $\overline{S}^* = \frac{1}{G(0)}$, is satisfied, a fact which completes the proof.

Invariant region

The concept of invariant region is of great importance in the theory of dynamical systems since this region plays an essential part in various situations in which the behaviour of the solution is restrained. For the biological system (5) under consideration, the state variables denote the populations of susceptible, infected,

diagnosed, ailing, recognized, infected real, threatened, diagnosed recovered, healed, and extinct people, all of which are non-negative and bounded quantities. Therefore, the non-negativity and bounded-ness of the solution is an important property, which is needed for the proposed model in order to be realistic and biologically meaningful. To achieve this aim, here we show that the system (5) lies in the positive region $\mathbb{R}_+^{10}$, which means that $\mathbb{R}_+^{10}$ is a positively invariant set for the dynamical system (5); that is, any solution trajectory starting from $\mathbb{R}_+^{10}$ will stay in this region for all future time. Therefore, the existence of invariant region $\mathbb{R}_+^{10}$ for the state space of our model entails a non-negative bound on the solution's behaviour. As a result, the validation of priori specified constraints on the model (5) is confirmed with the help of this invariant set. To show that the solution of the system (5) along with its DFE is non-negative in the region $\mathbb{R}_+^{10}$, we start with the first class $S(t)$ by

$$
\mathscr{D}_t^q S(t) = -(\alpha^q I(t) + \beta^q D(t) + \gamma^q A(t) + \delta^q R(t))S(t).
\tag{37}
$$

Thus, at the DFE, we have

$$
\mathscr{D}_t^q S(t) = 0 \geqslant 0.
\tag{38}
$$

Similarly, for the next classes $I(t)$ and $D(t)$ at the DFE, we, respectively, get

$$
\mathscr{D}_t^q I(t) = 0 \geqslant 0,
\tag{39}
$$

and

$$
\mathscr{D}_t^q D(t) = \epsilon^q I(t) \geqslant 0.
\tag{40}
$$

Since all parameters used in model are non-negative, $D(t)$ is also positive for all $t \geqslant 0$. Following the same strategy for the other variables, we can write

$$
\begin{aligned}
\mathscr{D}_t^q A(t) &= \zeta^q I(t) \geqslant 0, \\
\mathscr{D}_t^q R(t) &= \eta^q D(t) + \theta^q A(t) \geqslant 0, \\
\mathscr{D}_t^q I_r(t) &= (\alpha^q I(t) + \beta^q D(t) + \gamma^q A(t) + \delta^q R(t))S(t) \geqslant 0, \\
\mathscr{D}_t^q T(t) &= \mu^q A(t) + v^q R(t) \geqslant 0, \\
\mathscr{D}_t^q H_d(t) &= \rho^q D(t) + \xi^q R(t) + \sigma^q T(t) \geqslant 0, \\
\mathscr{D}_t^q H(t) &= \lambda^q I(t) + \rho^q D(t) + \kappa^q A(t) + \xi^q R(t) + \sigma^q T(t) \geqslant 0, \\
\mathscr{D}_t^q E(t) &= \tau^q T(t) \geqslant 0.
\end{aligned}
\tag{41}
$$

Hence, all equations give non-negative values. As a result, the system (5) lies in the non-negative region $\mathbb{R}_+^{10}$.

Basic reproduction number

Consider the five infected compartments and reduce the model (5) to a matrix form as below

$$\mathscr{D}_t^q X(t) = W_1(t) - W_2(t), \tag{42}$$

where $X(t) = [I(t) \quad D(t) \quad A(t) \quad R(t) \quad T(t)]^T$,

$$W_1(t) = \begin{bmatrix} \alpha^q S & \beta^q S & \gamma^q S & \delta^q R & 0 \\ 0 & 0 & 0 & 0 & 0 \\ 0 & 0 & 0 & 0 & 0 \\ 0 & 0 & 0 & 0 & 0 \\ 0 & 0 & 0 & 0 & 0 \end{bmatrix}, \tag{43}$$

$$W_2(t) = \begin{bmatrix} \omega_1 & 0 & 0 & 0 & 0 \\ -\xi & \omega_2 & 0 & 0 & 0 \\ -\epsilon^q & 0 & \omega_3 & 0 & 0 \\ 0 & -\theta^q & -\eta^q & \omega_4 & 0 \\ 0 & -\mu^q & 0 & -v^q & \omega_5 \end{bmatrix}, \tag{44}$$

and

$$W_2^{-1}(t) = \begin{bmatrix} \frac{1}{\omega_1} & 0 & 0 & 0 & 0 \\ \frac{\xi}{\omega_1\omega_2} & \frac{1}{\omega_2} & 0 & 0 & 0 \\ \frac{\epsilon}{\omega_1\omega_3} & 0 & \frac{1}{\omega_3} & 0 & 0 \\ \frac{\xi\theta\omega_3+\epsilon\eta\omega_2}{\omega_1\omega_2\omega_3\omega_4} & \frac{\theta}{\omega_2\omega_4} & \frac{\eta}{\omega_3\omega_4} & \frac{1}{\omega_4} & 0 \\ \frac{\xi\theta v\omega_3+\xi\mu\omega_3\omega_4+v\eta\epsilon\omega_2}{\omega_1\omega_2\omega_3\omega_4\omega_5} & \frac{\theta v+\mu\omega_4}{\omega_2\omega_4\omega_5} & \frac{v\eta}{\omega_3\omega_4\omega_5} & \frac{v}{\omega_4\omega_5} & \frac{1}{\omega_5} \end{bmatrix}. \tag{45}$$

The spectral radius of $W_1 W_2^{-1}$ is equal to $\mathfrak{R}_0$; this gives the basic reproduction number as

$$\mathfrak{R}_0 = \left(\frac{\delta^q\theta^q\xi}{\omega_1\omega_3\omega_4} + \frac{\delta^q\epsilon^q\eta^q}{\omega_1\omega_2\omega_4} + \frac{v^q\xi}{\omega_1\omega_3} + \frac{\beta^q\epsilon^q}{\omega_1\omega_2} + \frac{\alpha^q}{\omega_1} \right) S. \tag{46}$$

Global stability

For the global stability, if $\mathfrak{R}_0 < 1$, then an infected person transfers the disease individually to less than one newly infected person on average over the lifetime of his/her infectious time, so the infection cannot spread. On the other hand, at an endemic equilibrium point when $\mathfrak{R}_0 > 1$, the disease is transferred from each infected person to more than one susceptible persons on average, so the disease spreads across the population. In the following, we will prove this mathematically.

Theorem 4. If $\mathfrak{R}_0 < 1$, then the DFE is globally stable, else it is unstable.

Proof. To prove this theorem, we employ a Lyapunov function whose fractional derivative is defined by

$$\mathscr{D}_t^q V(t) = \frac{1}{\omega_1}\mathscr{D}_t^q I(t) + \frac{1}{\omega_2}\mathscr{D}_t^q D(t) + \frac{1}{\omega_3}\mathscr{D}_t^q A(t) + \frac{1}{\omega_4}\mathscr{D}_t^q R(t)$$
$$+ \frac{1}{\omega_5}\mathscr{D}_t^q T(t). \tag{47}$$

By using the fractional model (5), we get

$$
\begin{aligned}
\mathscr{D}_t^q V(t) = \ & \frac{1}{\omega_1}[-\omega_1 I(t) + \alpha^q I(t)S(t) + \beta^q D(t)S(t) + \gamma^q A(t)S(t) + \delta^q R(t)S(t)] + \frac{1}{\omega_2}[-\omega_2 D(t) + \epsilon^q I(t)] \\
& + \frac{1}{\omega_3}[-\omega_3 A(t) + \zeta^q I(t)] + \frac{1}{\omega_4}[-\omega_4 R(t) + \eta^q D(t) + \theta^q A(t)] + \frac{1}{\omega_5}[-\omega_5 T(t) + \mu^q A(t) + v^q R(t)] \\
= \ & \frac{1}{\omega_1}[\alpha^q I(t)S(t) + \beta^q D(t)S(t) + \gamma^q A(t)S(t) + \delta^q R(t)S(t)] - I(t) + \frac{1}{\omega_2}[\epsilon^q I(t)] - D(t) \\
& + \frac{1}{\omega_3}[\zeta^q I(t)] - A(t) + \frac{1}{\omega_4}[\eta^q D(t) + \theta^q A(t)] - R(t) + \frac{1}{\omega_5}[\mu^q A(t) + v^q R(t)] - T(t) \\
= \ & \frac{1}{\omega_1}[\alpha^q I(t)S(t) + \beta^q D(t)S(t) + \gamma^q A(t)S(t) + \delta^q R(t)S(t)] + \frac{1}{\omega_2}[\epsilon^q I(t)] + \frac{1}{\omega_3}[\zeta^q I(t)] \\
& + \frac{1}{\omega_4}[\eta^q D(t) + \theta^q A(t)] + \frac{1}{\omega_5}[\mu^q A(t) + v^q R(t)] - [T(t) + R(t) + A(t) + D(t) + I(t)] \\
= \ & \left[\frac{1}{T(t)+R(t)+A(t)+D(t)+I(t)} \left[\frac{1}{\omega_1}[\alpha^q I(t)S(t) + \beta^q D(t)S(t) + \gamma^q A(t)S(t) + \delta^q R(t)S(t)] \right. \right. \\
& + \frac{1}{\omega_2}[\epsilon^q I(t)] + \frac{1}{\omega_3}[\zeta^q I(t)] + \frac{1}{\omega_4}[\eta^q D(t) + \theta^q A(t)] \\
& \left. \left. + \frac{1}{\omega_5}[\mu^q A(t) + v^q R(t)] \right] - 1 \right][T(t) + R(t) + A(t) + D(t) + I(t)] \\
\leqslant \ & (\mathfrak{R}_0 - 1)[T(t) + R(t) + A(t) + D(t) + I(t)].
\end{aligned}
\tag{48}
$$

Therefore, the condition $\mathfrak{R}_0 < 1$ implies that $D_t^q \mathscr{D}_t^q V(t) \leq 0$. Thus, the proof is complete.

Numerical method

By applying the Laplace transform to the both sides of the system (5), we have

$$
\begin{aligned}
&\mathscr{L}\left[\mathscr{D}_t^q S(t)\right] = -\alpha^q \mathscr{L}[I(t)S(t)] - \beta^q \mathscr{L}[D(t)S(t)] - \gamma^q \mathscr{L}[A(t)S(t)] - \delta^q \mathscr{L}[R(t)S(t)], \\
&\mathscr{L}\left[\mathscr{D}_t^q I(t)\right] = -\omega_1 \mathscr{L}[I(t)] + \alpha^q \mathscr{L}[I(t)S(t)] + \beta^q \mathscr{L}[D(t)S(t)] + \gamma^q \mathscr{L}[A(t)S(t)] + \delta^q \mathscr{L}[R(t)S(t)], \\
&\mathscr{L}\left[\mathscr{D}_t^q D(t)\right] = -\omega_2 \mathscr{L}[D(t)] + \epsilon^q \mathscr{L}[I(t)], \\
&\mathscr{L}\left[\mathscr{D}_t^q A(t)\right] = -\omega_3 \mathscr{L}[A(t)] + \zeta^q \mathscr{L}[I(t)], \\
&\mathscr{L}\left[\mathscr{D}_t^q R(t)\right] = -\omega_4 \mathscr{L}[R(t)] + \eta^q \mathscr{L}[D(t)], \\
&\mathscr{L}\left[\mathscr{D}_t^q I_r(t)\right] = \alpha^q \mathscr{L}[I(t)S(t)] + \beta^q \mathscr{L}[D(t)S(t)] + \gamma^q \mathscr{L}[A(t)S(t)] + \delta^q \mathscr{L}[R(t)S(t)], \\
&\mathscr{L}\left[\mathscr{D}_t^q T(t)\right] = -\omega_5 \mathscr{L}[T(t)] + \mu^q \mathscr{L}[A(t)] + \nu^q \mathscr{L}[R(t)], \\
&\mathscr{L}\left[\mathscr{D}_t^q H_d(t)\right] = \rho \mathscr{L}[D(t)] + \xi \mathscr{L}[R(t)] + \sigma \mathscr{L}[T(t)], \\
&\mathscr{L}\left[\mathscr{D}_t^q H(t)\right] = \lambda^q \mathscr{L}[I(t)] + \rho \mathscr{L}[D(t)] + \kappa \mathscr{L}[A(t)] + \sigma \mathscr{L}[T(t)], \\
&\mathscr{L}\left[\mathscr{D}_t^q E(t)\right] = \tau^q \mathscr{L}[T(t)].
\end{aligned}
\tag{49}
$$

Using the definition of Laplace transform for the Caputo fractional derivative, we derive

$$
\begin{aligned}
&s^q\left(\mathscr{L}[S(t)] - \tfrac{S(0)}{s}\right) = -\alpha^q \mathscr{L}[I(t)S(t)] - \beta^q \mathscr{L}[D(t)S(t)] - \gamma^q \mathscr{L}[A(t)S(t)] - \delta^q \mathscr{L}[R(t)S(t)], \\
&s^q\left(\mathscr{L}[I(t)] - \tfrac{I(0)}{s}\right) = -\omega_1 \mathscr{L}[I(t)] + \alpha^q \mathscr{L}[I(t)S(t)] + \beta^q \mathscr{L}[D(t)S(t)] + \gamma^q \mathscr{L}[A(t)S(t)] + \delta^q \mathscr{L}[R(t)S(t)], \\
&s^q\left(\mathscr{L}[D(t)] - \tfrac{D(0)}{s}\right) = -\omega_2 \mathscr{L}[D(t)] + \epsilon^q \mathscr{L}[I(t)], \\
&s^q\left(\mathscr{L}[A(t)] - \tfrac{A(0)}{s}\right) = -\omega_3 \mathscr{L}[A(t)] + \zeta^q \mathscr{L}[I(t)], \\
&s^q\left(\mathscr{L}[R(t)] - \tfrac{R(0)}{s}\right) = -\omega_4 \mathscr{L}[R(t)] + \eta^q \mathscr{L}[D(t)], \\
&s^q\left(\mathscr{L}[I_r(t)] - \tfrac{I_r(0)}{s}\right) = \alpha^q \mathscr{L}[I(t)S(t)] + \beta^q \mathscr{L}[D(t)S(t)] + \gamma^q \mathscr{L}[A(t)S(t)] + \delta^q \mathscr{L}[R(t)S(t)], \\
&s^q\left(\mathscr{L}[T(t)] - \tfrac{T(0)}{s}\right) = -\omega_5 \mathscr{L}[T(t)] + \mu^q \mathscr{L}[A(t)] + \nu^q \mathscr{L}[R(t)], \\
&s^q\left(\mathscr{L}[H_d(t)] - \tfrac{H_d(0)}{s}\right) = \rho \mathscr{L}[D(t)] + \xi \mathscr{L}[R(t)] + \sigma \mathscr{L}[T(t)], \\
&s^q\left(\mathscr{L}[H(t)] - \tfrac{H(0)}{s}\right) = \lambda^q \mathscr{L}[I(t)] + \rho \mathscr{L}[D(t)] + \kappa \mathscr{L}[A(t)] + \sigma \mathscr{L}[T(t)], \\
&s^q\left(\mathscr{L}[E(t)] - \tfrac{E(0)}{s}\right) = \tau^q \mathscr{L}[T(t)].
\end{aligned}
\tag{50}
$$

With a simple manipulation, we obtain

$$
\begin{aligned}
\mathscr{L}[S(t)] &= \frac{S(0)}{s} + \frac{-\alpha^q \mathscr{L}[I(t)S(t)] - \beta^q \mathscr{L}[D(t)S(t)] - \gamma^q \mathscr{L}[A(t)S(t)] - \delta^q \mathscr{L}[R(t)S(t)]}{s^q}, \\
\mathscr{L}[I(t)] &= \frac{I(0)}{s} + \frac{-\omega_1 \mathscr{L}[I(t)] + \alpha^q \mathscr{L}[I(t)S(t)] + \beta^q \mathscr{L}[D(t)S(t)] + \gamma^q \mathscr{L}[A(t)S(t)] + \delta^q \mathscr{L}[R(t)S(t)]}{s^q}, \\
\mathscr{L}[D(t)] &= \frac{D(0)}{s} + \frac{-\omega_2 \mathscr{L}[D(t)] + \epsilon^q \mathscr{L}[I(t)]}{s^q}, \\
\mathscr{L}[A(t)] &= \frac{A(0)}{s} + \frac{-\omega_3 \mathscr{L}[A(t)] + \zeta^q \mathscr{L}[I(t)]}{s^q}, \\
\mathscr{L}[R(t)] &= \frac{R(0)}{s} + \frac{-\omega_4 \mathscr{L}[R(t)] + \eta^q \mathscr{L}[D(t)]}{s^q}, \\
\mathscr{L}[I_r(t)] &= \frac{I_r(0)}{s} + \frac{\alpha^q \mathscr{L}[I(t)S(t)] + \beta^q \mathscr{L}[D(t)S(t)] + \gamma^q \mathscr{L}[A(t)S(t)] + \delta^q \mathscr{L}[R(t)S(t)]}{s^q}, \\
\mathscr{L}[T(t)] &= \frac{T(0)}{s} + \frac{-\omega_5 \mathscr{L}[T(t)] + \mu^q \mathscr{L}[A(t)] + v^q \mathscr{L}[R(t)]}{s^q}, \\
\mathscr{L}[H_d(t)] &= \frac{H_d(0)}{s} + \frac{\rho \mathscr{L}[D(t)] + \xi \mathscr{L}[R(t)] + \sigma \mathscr{L}[T(t)]}{s^q}, \\
\mathscr{L}[H(t)] &= \frac{H(0)}{s} + \frac{\lambda^q \mathscr{L}[I(t)] + \rho \mathscr{L}[D(t)] + \kappa \mathscr{L}[A(t)] + \sigma \mathscr{L}[T(t)]}{s^q}, \\
\mathscr{L}[E(t)] &= \frac{E(0)}{s} + \frac{\tau^q \mathscr{L}[T(t)]}{s^q},
\end{aligned}
\tag{51}
$$

where the state variables at $t = 0$ are the initial conditions. Let us assume that the solutions are in the form

$$
\begin{aligned}
& S(t) = \sum_{k=0}^{\infty} S_k(t), \; I(t) = \sum_{k=0}^{\infty} I_k(t), \; D(t) = \sum_{k=0}^{\infty} D_k(t), \\
& A(t) = \sum_{k=0}^{\infty} A_k(t), \; R(t) = \sum_{k=0}^{\infty} R_k(t), \\
& I_r(t) = \sum_{k=0}^{\infty} I_{r,k}(t), \; T(t) = \sum_{k=0}^{\infty} T_k(t), \; H_d(t) = \sum_{k=0}^{\infty} H_{d,k}(t), \\
& H(t) = \sum_{k=0}^{\infty} H_k(t), \; E(t) = \sum_{k=0}^{\infty} E_k(t).
\end{aligned}
\tag{52}
$$

Then the non-linear terms in the model can be written as

$$
\begin{aligned}
I(t)S(t) &= \sum_{k=0}^{\infty} G_k(t), \; D(t)S(t) = \sum_{k=0}^{\infty} H_k(t), \; A(t)S(t) \\
&= \sum_{k=0}^{\infty} P_k(t), \; R(t)S(t) = \sum_{k=0}^{\infty} Q_k(t),
\end{aligned}
\tag{53}
$$

where G_k, H_k, P_k and Q_k are called Adomian polynomials. Now, we provide the following results

$$
\begin{aligned}
& \mathscr{L}[S_0(t)] = \frac{S(0)}{s}, \; \mathscr{L}[I_0(t)] = \frac{I(0)}{s}, \; \mathscr{L}[D_0(t)] = \frac{D(0)}{s}, \\
& \mathscr{L}[A_0(t)] = \frac{A(0)}{s}, \; \mathscr{L}[R_0(t)] = \frac{R(0)}{s}, \\
& \mathscr{L}[I_{r,0}(t)] = \frac{I_r(0)}{s}, \; \mathscr{L}[T_0(t)] = \frac{T(0)}{s}, \; \mathscr{L}[H_{d,0}] = \frac{H_d(0)}{s}, \\
& \mathscr{L}[H_0(t)] = \frac{H(0)}{s}, \; \mathscr{L}[E_0(t)] = \frac{E(0)}{s}.
\end{aligned}
\tag{54}
$$

Using the above expressions, we have the following first-order approximations

$$
\begin{aligned}
\mathscr{L}[S_1(t)] &= \frac{-\alpha^q \mathscr{L}[G_0(t)] - \beta^q \mathscr{L}[H_0(t)] - \gamma^q \mathscr{L}[P_0(t)] - \delta^q \mathscr{L}[Q_0(t)]}{s^q}, \\
\mathscr{L}[I_1(t)] &= \frac{-\omega_1 \mathscr{L}[I_0(t)] + \alpha^q \mathscr{L}[G_0(t)] + \beta^q \mathscr{L}[H_0(t)] + \gamma^q \mathscr{L}[P_0(t)] + \delta^q \mathscr{L}[Q_0(t)]}{s^q}, \\
\mathscr{L}[D_1(t)] &= \frac{-\omega_2 \mathscr{L}[D_0(t)] + \epsilon^q \mathscr{L}[I_0(t)]}{s^q}, \\
\mathscr{L}[A_1(t)] &= \frac{-\omega_3 \mathscr{L}[A_0(t)] + \zeta^q \mathscr{L}[I_0(t)]}{s^q}, \\
\mathscr{L}[R_1(t)] &= \frac{-\omega_4 \mathscr{L}[R_0(t)] + \eta^q \mathscr{L}[D_0(t)]}{s^q}, \\
\mathscr{L}[I_{r,1}(t)] &= \frac{\alpha^q \mathscr{L}[G_0(t)] + \beta^q \mathscr{L}[H_0(t)] + \gamma^q \mathscr{L}[P_0(t)] + \delta^q \mathscr{L}[Q_0(t)]}{s^q}, \\
\mathscr{L}[T_1(t)] &= \frac{-\omega_5 \mathscr{L}[T_0(t)] + \mu^q \mathscr{L}[A_0(t)] + v^q \mathscr{L}[R_0(t)]}{s^q}, \\
\mathscr{L}[H_{d,1}(t)] &= \frac{\rho \mathscr{L}[D_0(t)] + \xi \mathscr{L}[R_0(t)] + \sigma \mathscr{L}[T_0(t)]}{s^q}, \\
\mathscr{L}[H_1(t)] &= \frac{\lambda^q \mathscr{L}[I_0(t)] + \rho \mathscr{L}[D_0(t)] + \kappa \mathscr{L}[A_0(t)] + \sigma \mathscr{L}[T_0(t)]}{s^q}, \\
\mathscr{L}[E_1(t)] &= \frac{\tau^q \mathscr{L}[T_0(t)]}{s^q}.
\end{aligned}
\tag{55}
$$

Similarly, we get a generalized form for the numerical solution as below

$$
\begin{aligned}
\mathscr{L}[S_{k+1}(t)] &= \frac{-\alpha^q \mathscr{L}[G_k(t)] - \beta^q \mathscr{L}[H_k(t)] - \gamma^q \mathscr{L}[P_k(t)] - \delta^q \mathscr{L}[Q_k(t)]}{s^q}, \\
\mathscr{L}[I_{k+1}(t)] &= \frac{-\omega_1 \mathscr{L}[I_k(t)] + \alpha^q \mathscr{L}[G_k(t)] + \beta^q \mathscr{L}[H_k(t)] + \gamma^q \mathscr{L}[P_k(t)] + \delta^q \mathscr{L}[Q_k(t)]}{s^q}, \\
\mathscr{L}[D_{k+1}(t)] &= \frac{-\omega_2 \mathscr{L}[D_k(t)] + \epsilon^q \mathscr{L}[I_k(t)]}{s^q}, \\
\mathscr{L}[A_{k+1}(t)] &= \frac{-\omega_3 \mathscr{L}[A_k(t)] + \zeta^q \mathscr{L}[I_k(t)]}{s^q}, \\
\mathscr{L}[R_{k+1}(t)] &= \frac{-\omega_4 \mathscr{L}[R_k(t)] + \eta^q \mathscr{L}[D_k(t)]}{s^q}, \\
\mathscr{L}[I_{r,k+1}(t)] &= \frac{\alpha^q \mathscr{L}[G_k(t)] + \beta^q \mathscr{L}[H_k(t)] + \gamma^q \mathscr{L}[P_k(t)] + \delta^q \mathscr{L}[Q_k(t)]}{s^q}, \\
\mathscr{L}[T_{k+1}(t)] &= \frac{-\omega_5 \mathscr{L}[T_k(t)] + \mu^q \mathscr{L}[A_k(t)] + v^q \mathscr{L}[R_k(t)]}{s^q}, \\
\mathscr{L}[H_{d,k+1}(t)] &= \frac{\rho \mathscr{L}[D_k(t)] + \xi \mathscr{L}[R_k(t)] + \sigma \mathscr{L}[T_k(t)]}{s^q}, \\
\mathscr{L}[H_{k+1}(t)] &= \frac{\lambda^q \mathscr{L}[I_k(t)] + \rho \mathscr{L}[D_k(t)] + \kappa \mathscr{L}[A_k(t)] + \sigma \mathscr{L}[T_k(t)]}{s^q}, \\
\mathscr{L}[E_{k+1}(t)] &= \frac{\tau^q \mathscr{L}[T_k(t)]}{s^q}.
\end{aligned}
\tag{56}
$$

The convergence analysis of the presented numerical technique is established by the following theorem:

Theorem 5. [34] Let $\mathbb{X}$ be a Banach space and $G : \mathbb{X} \to \mathbb{X}$ be a contraction operator such that $\forall y, \bar{y} \in \mathbb{X}, \|Gy - G\bar{y}\| \leqslant \beta \|y - \bar{y}\|, 0 < \beta < 1$. Now, if we generate the series in (52) by the method (55)–(56) as

$$
y_k = G y_{k-1}, \quad y_{k-1} = \sum_{i=0}^{k-1} y_i, \quad k = 1, 2, 3, \ldots,
\tag{57}
$$

and if $y_0 \in \mathbb{A}_\varrho(y)$ where $\mathbb{A}_\varrho(y) = \{\bar{y} \in \mathbb{X} : \|\bar{y} - y\| < \varrho\}$, then

$(i) y_k \in \mathbb{A}_\varrho(y)$

$(ii) \lim_{k \to \infty} y_k = y.$

Proof. (i) Using mathematical induction, for $k = 1$ we have

$$
\|y_1 - y\| = \|G y_0 - G y\| \leqslant \beta \|y_0 - y\|.
\tag{58}
$$

Let the result be true for $k - 1$; then

$$
\|y_{k-1} - y\| \leqslant \beta^{k-1} \|y_0 - y\|.
\tag{59}
$$

Continuing as above, we attain

$$
\|y_k - y\| = \|G y_{k-1} - G y\| \leqslant \beta \|y_{k-1} - y\| \leqslant \beta^k \|y_0 - y\|.
\tag{60}
$$

Hence, we get

$$
\|y_k - y\| \leqslant \beta^k \|y_0 - y\| \leqslant \beta^k \varrho < \varrho,
\tag{61}
$$

which implies that $y_k \in \mathbb{A}_\varrho(y)$.

(ii) As $\|y_k - y\| \leqslant \beta^k \|y_0 - y\|$ and since $\lim_{k \to \infty} \beta^k = 0$, we have $\lim_{k \to \infty} \|y_k - y\| \to 0$, which concludes that $\lim_{k \to \infty} y_k = y$.

Simulation results

In this part, we apply the approximation scheme, developed in the previous section, to investigate the generalized fractional model (5). The values of parameters and coefficients for the model (5) are given in the Table 1, computed by the following data-fitting technique. Indeed, we fixed the fractional order as $q = 1$ and employed a least-squares fitting scheme to simulate the results and evaluate the parameters according to the real COVID-19 cases in Italy [30].

Simulation results for different fractional orders are given in Figs. 2–6. As can be seen, the fractional model (5) has a flexible structure due to the existence of its fractional order parameter, so it has the potential of extracting the hidden aspects of the real case study under investigation more accurately than the existing classical framework. The presented simulation curves in Figs. 2–6

Table 1
Descriptions and values of parameters.

Symbol	Description	Value
α	Transmission rate owing to the connection with unrecognized asymptomatic patients	0.57
β	Transmission rate owing to the connection with recognized asymptomatic patients	0.0114
γ	Transmission rate owing to the connection with unrecognized symptomatic patients	0.456
δ	Transmission rate owing to the connection with recognized symptomatic patients	0.0114
ϵ	Asymptomatic detection rate	0.171
θ	Symptomatic detection rate	0.3705
ζ	Transmission rate of unrecognized asymptomatic patients into infected ones	0.1254
η	Transmission rate of recognized asymptomatic patients into infected ones	0.1254
μ	Creation rate of life-threatening by unrecognized symptomatic patients	0.0171
ν	Creation rate of life-threatening by recognized symptomatic patients	0.0274
τ	Mortality rate of infections with life-threatening signs	0.01
λ	Recovery rate of patients who are unrecognized asymptomatic infected	0.0342
ρ	Recovery rate of patients who are recognized asymptomatic infected	0.0342
κ	Recovery rate of patients who are unrecognized symptomatic infected	0.0171
ξ	Recovery rate of patients who are recognized symptomatic infected	0.0171
σ	Recovery rate for the life-threatened symptomatic infected patients	0.0171

also describe that the people are assumed uninfected (susceptible) initially. When the outbreak first begins, the susceptible population starts declining steadily, as depicted in Fig. 2. Since they are exposed to infection, Figs. 3–6 show how quickly the population densities of infected and all other classes start growing. This increase causes the death rate to climb, but some people are recovered from the virus, so the number of people in both recovery and fatality groups are increased. Fig. 7 compares the numerical simulations with the real COVID-19 reported cases in Italy [30]. Besides, the absolute and relative errors for various fractional orders are computed in Table 2. Comparative results in Fig. 7 together with the error analysis in Table 2 show that the most accurate curves are achieved within the non-integer order $q = 0.99$; more importantly, the fractional response with $q = 0.99$ is obviously more precise than the classical one with $q = 1$. These advantages, as

mentioned above, are due to the fact that the fractional model exhibits a flexible structure to capture the real data by changing its fractional order. Consequently, the results in Fig. 7 and Table 2 justify the use of fractional calculus modelling approach over the available integer-order scheme to follow the reality very well, a fact which is due to the degree-of-freedom found in the fractional models and achieved by the fractional order parameter.

In order to predict and analyze the role of different parameters on the spread of viral infection, the transmission rates α and γ are varied, while keeping the fractional order as $q = 0.99$. The resulting behaviours of all system's compartments are plotted in Figs. 8–17. The effect of increasing the value of α from 0.57 to 0.67 is shown in Figs. 8–12. Fig. 8 implies that the transmission rate with unrecognized asymptomatic people should be reduced in order to control COVID-19 pandemic. Henceforth, keeping social distance is an effective strategy for the survival against this virus. According to Fig. 9, by increasing the amount of α, more people can be diagnosed who are asymptomatically infected, as compared to undetected symptomatically infected ones. The dynamics of recognized and currently infected people are presented in Fig. 10, which implies that the number of infected people is increased by increasing the transmission rate with unrecognized asymptomatic patients. Also, a greater number of symptomatic infected patients are detected earlier, which is helpful in taking precautionary measures beforehand. As a result, quarantining these patients could be a smart strategy to prevent future virus spread. Figs. 13–17 portray the effect of increasing the value of γ from 0.456 to 0.85. As can be seen from Fig. 13, the number of people infected from the virus is increased by increasing the transmission rate γ. Thus, in order to limit the COVID-19 pandemic, the transmission rate with undiagnosed symptomatic persons should be decreased. Keeping social isolation is, therefore, a good technique for surviving this infection. In comparison to undiagnosed symptomatically infected people, increasing the amount of γ allows more people to be diagnosed who are asymptomatically infected, according to Fig. 14. Fig. 15 depicts the dynamics of the identified and currently infected people. According to this figure, increasing the transmission rate with undiagnosed symptomatic individuals increases the number of infected people. In addition, a greater number of symptomatic infected patients is recognized earlier, allowing for early intervention. Thus, quarantining these patients could be an effective technique for preventing the virus propagation in the future. Furthermore, as shown in Fig. 16, the infected with life-threatening symptoms can be treated and recovered in a timely manner.
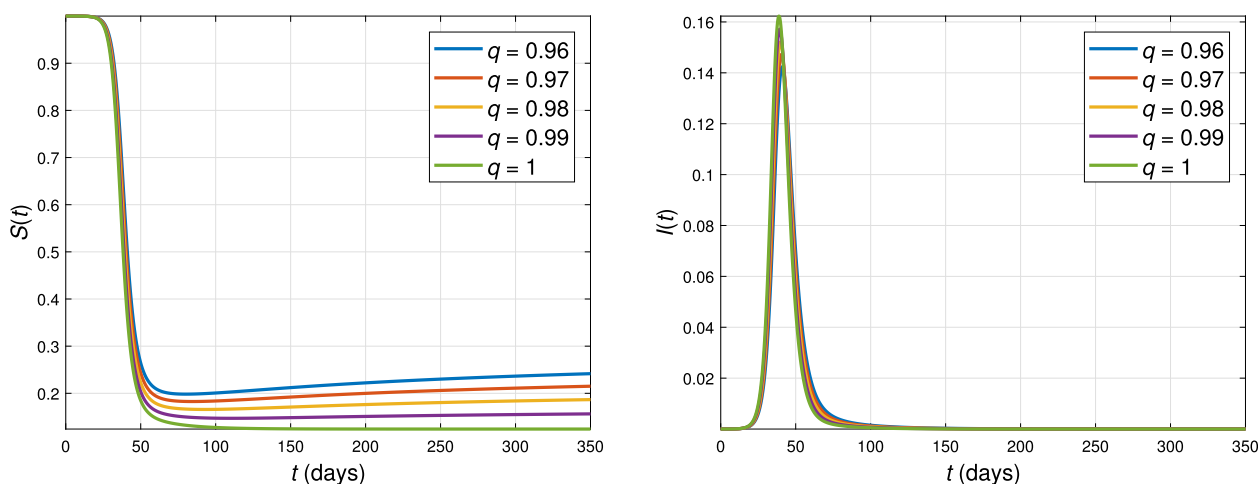

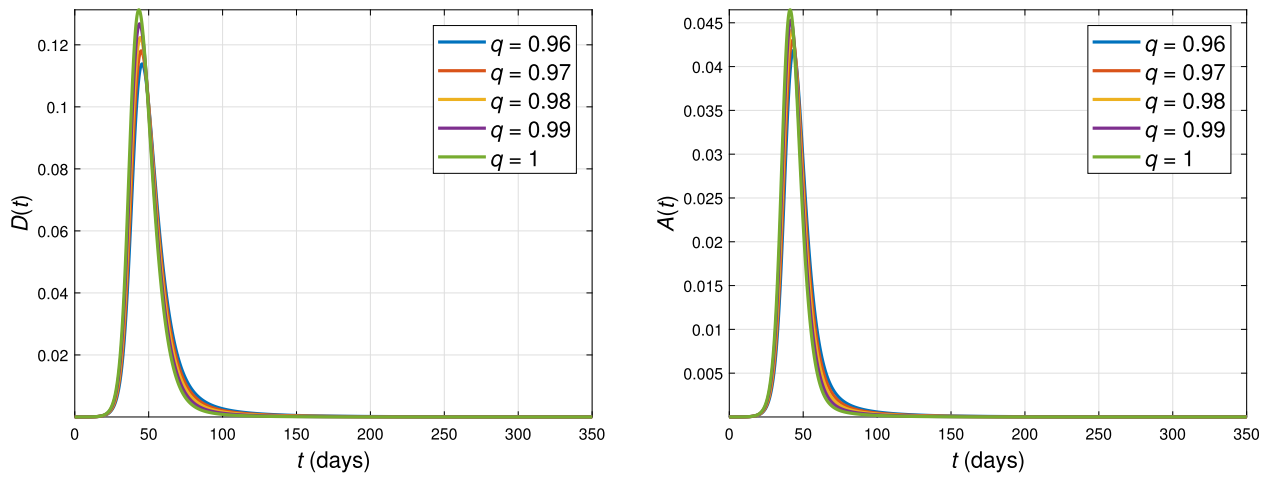**Fig. 2.** The state variables $S(t)$ and $I(t)$ for different fractional orders.

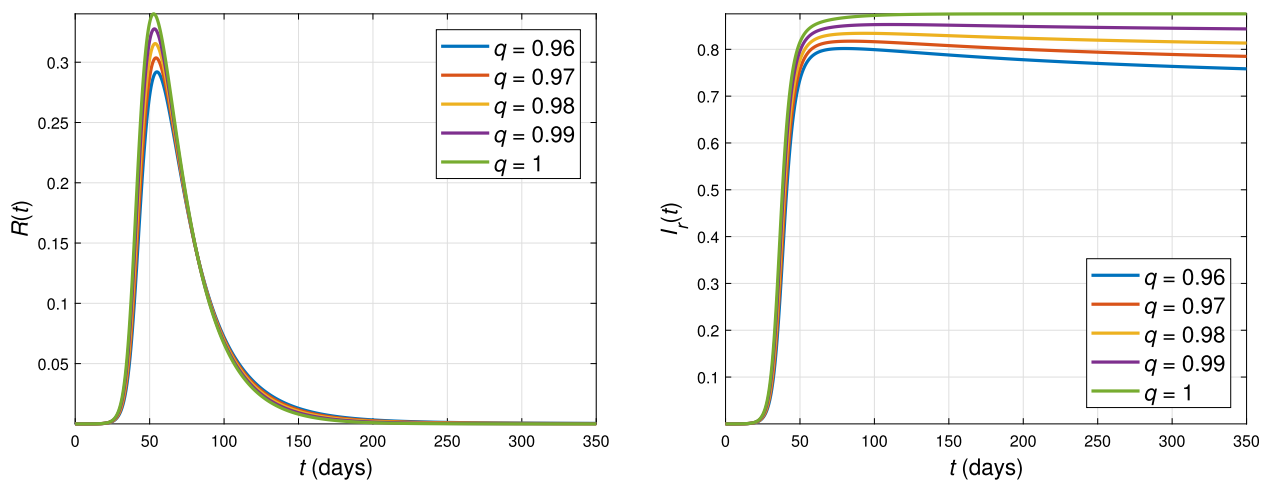**Fig. 3.** The state variables $D(t)$ and $A(t)$ for different fractional orders.

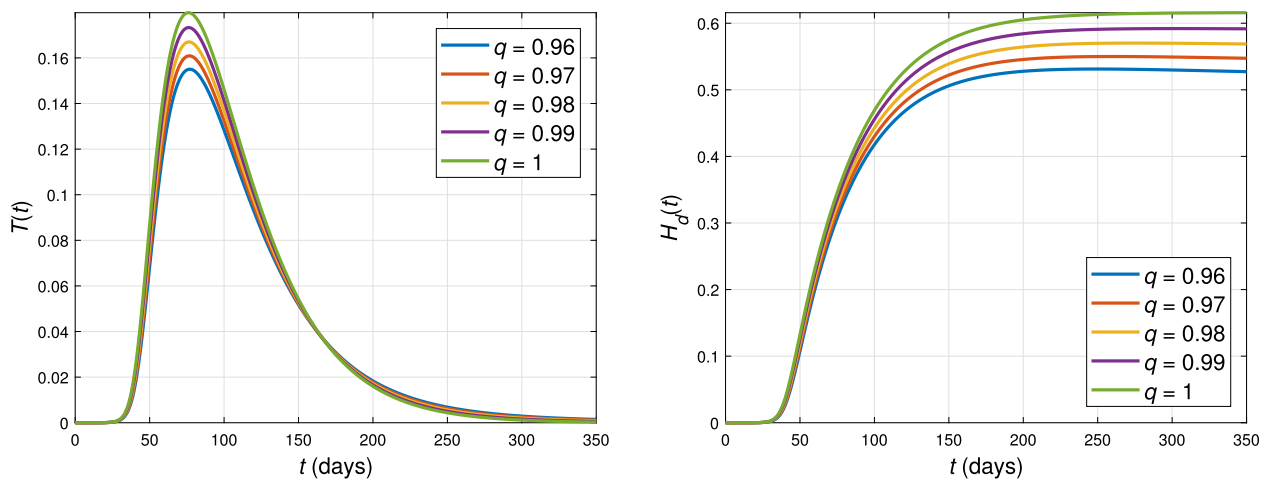**Fig. 4.** The state variables $R(t)$ and $I_r(t)$ for different fractional orders.

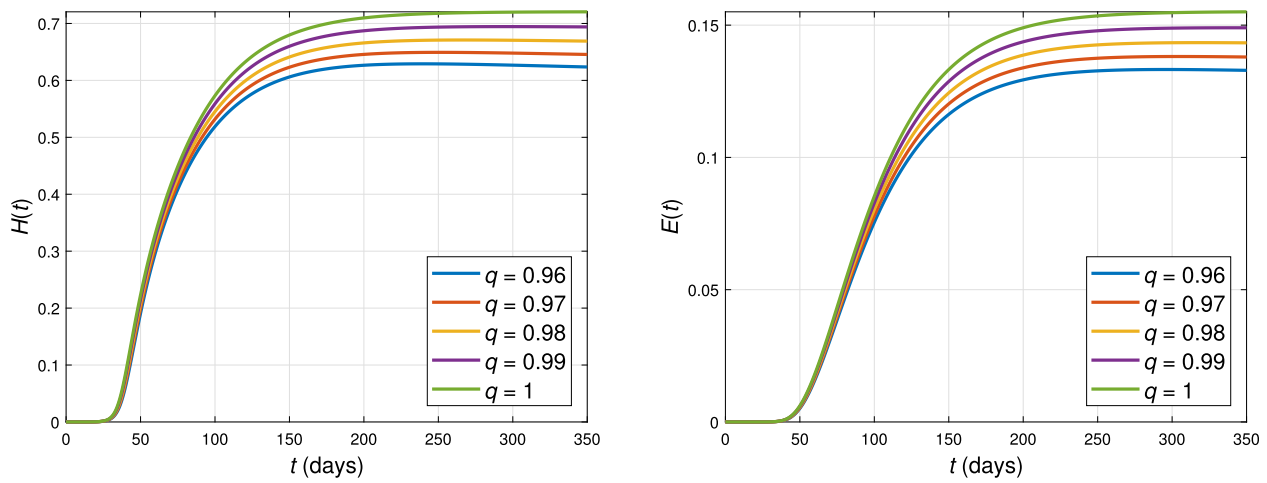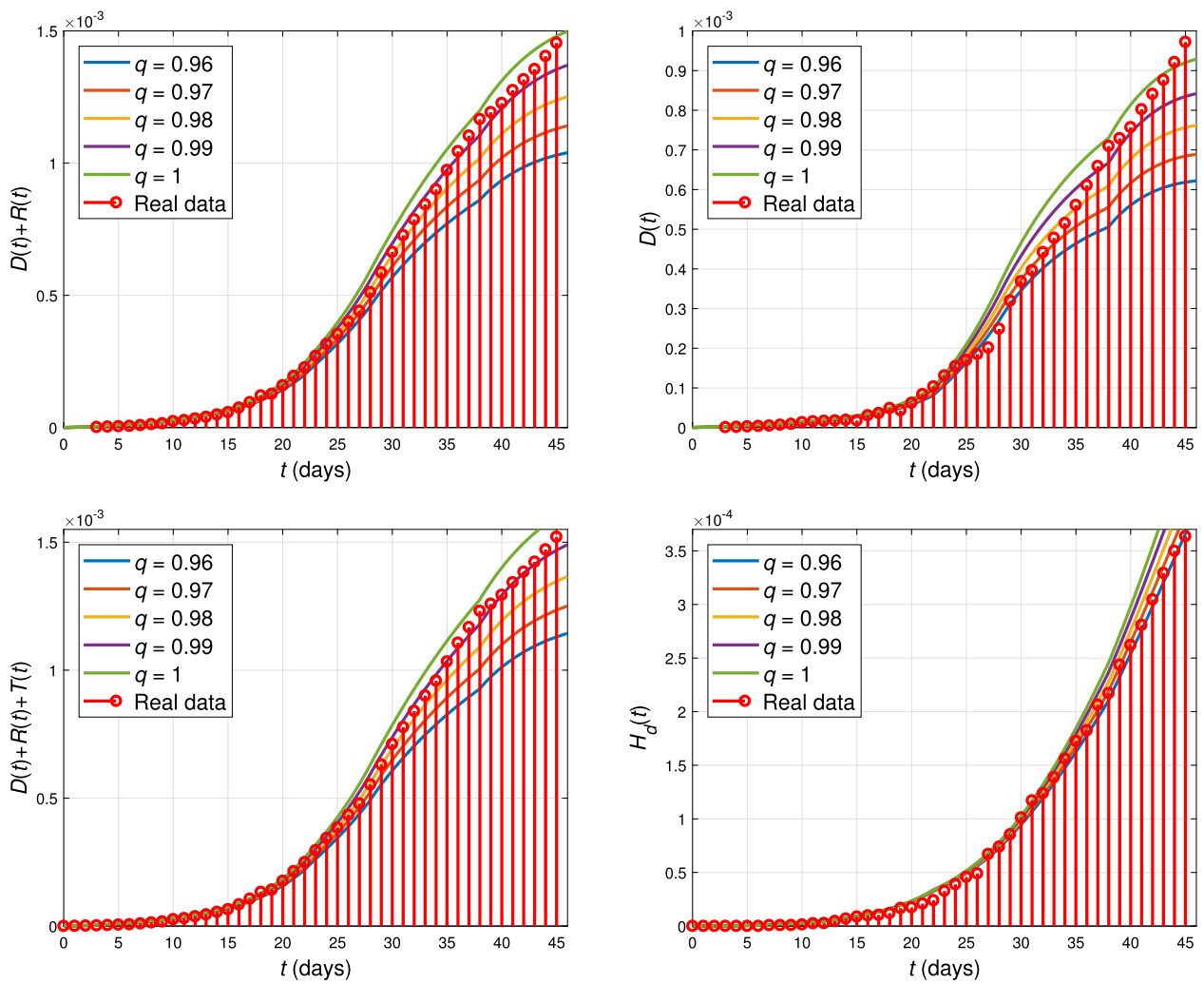**Fig. 5.** The state variables $T(t)$ and $H_d(t)$ for different fractional orders.

Fig. 6. The state variables $H(t)$ and $E(t)$ for different fractional orders.

Fig. 7. Simulation results versus real data.

Table 2
Absolute and relative errors for different fractional orders.

Fractional-order	Absolute error	Relative error
0.96	5.0338×10^4	0.0752
0.97	4.4278×10^4	0.0662
0.98	4.0401×10^4	0.0604
0.99	3.9253×10^4	0.0587
1	4.0988×10^4	0.0612

Conclusions

In this study, we introduced a Caputo-type fractional model to investigate the dynamics of COVID-19 pandemic and explore its fundamental behaviours. The new formulation employed a non-linear time-varying transmission rate and consisted of ten population classes. The existence and uniqueness results for the new model were discussed, and the associated dynamical characteristics including equilibrium points, invariant region, local and global stability, and basic reproduction number were examined.

Also, the values of coefficients and parameters were estimated by a data-fitting technique according to the real COVID-19 cases in Italy [30]. Numerical implementation was achieved by an efficient approximation scheme as the combination of Laplace transform and a successive substitution approach, and a convergence analysis was given for the considered method. Some figures were presented depicting the fractional results, which were compared with the aforementioned real COVID-19 reported cases. The best value of the fractional order with minimum relative and absolute errors was also found by using the above-mentioned comparative study. These comparisons, additionally, indicated that the non-integer order model follows the reality more precisely than the classical framework, a fact which justifies the use of fractional calculus modeling in our case under study. At the end, we analyzed the effect of transmission rates α and γ on the spread of viral infection, resulted in some useful intervention strategies. Future work can be focused on the examination of available control methodologies, such as optimal control [35,36], to see whether or not they could be helpful to eradicate this pandemic from communities.
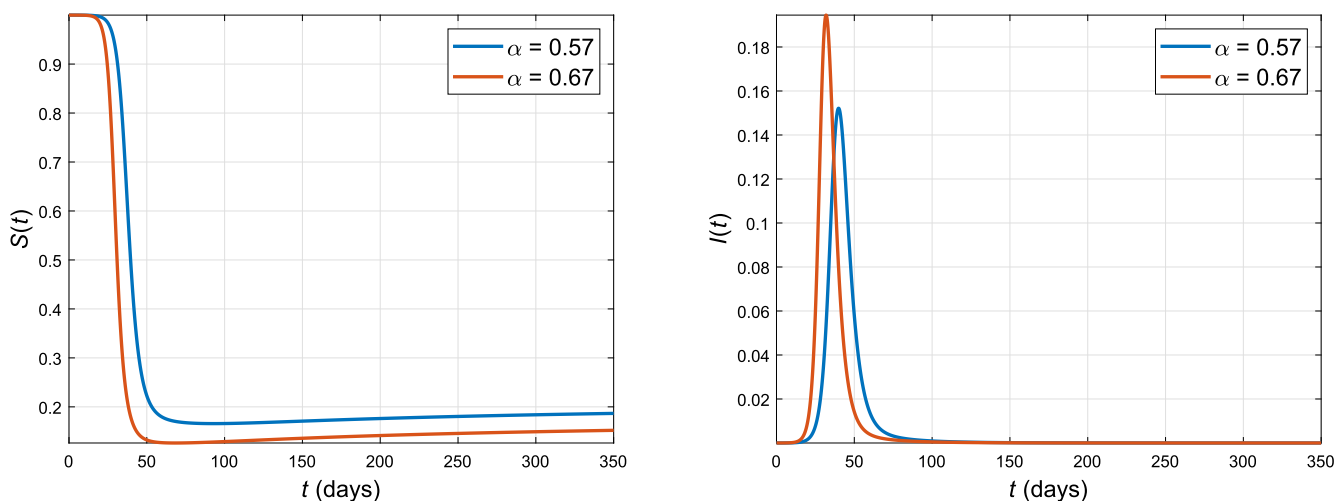

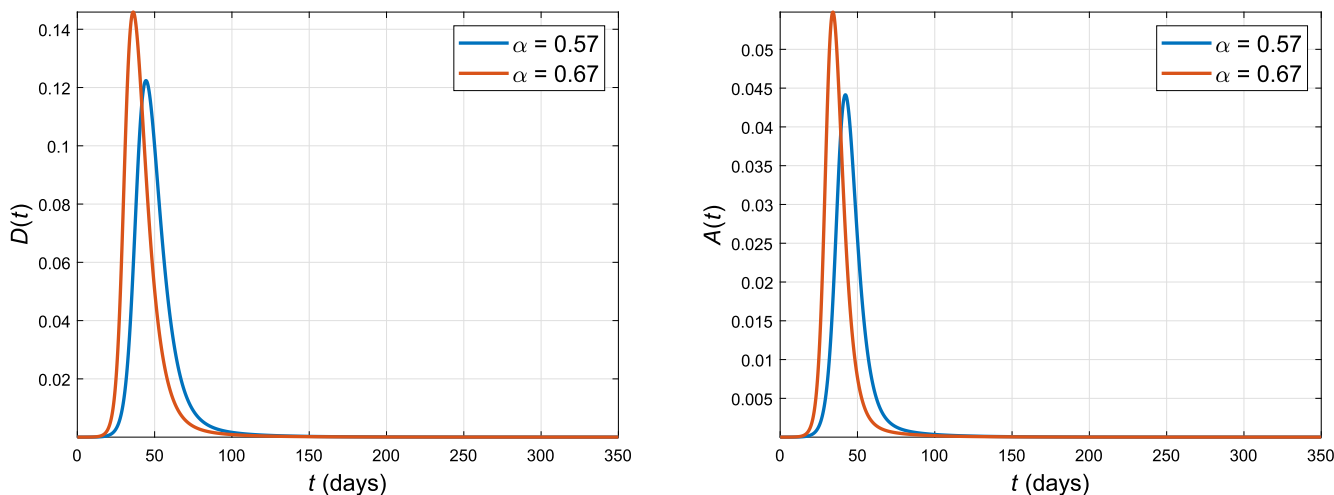**Fig. 8.** The state variables $S(t)$ and $I(t)$ for different values of α.

Fig. 9. The state variables $D(t)$ and $A(t)$ for different values of α.
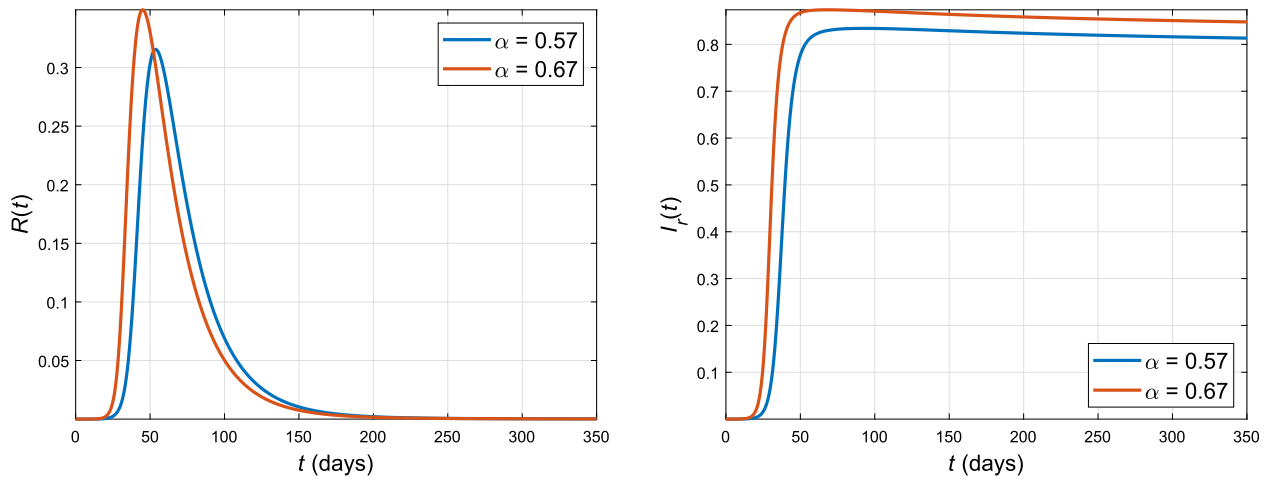
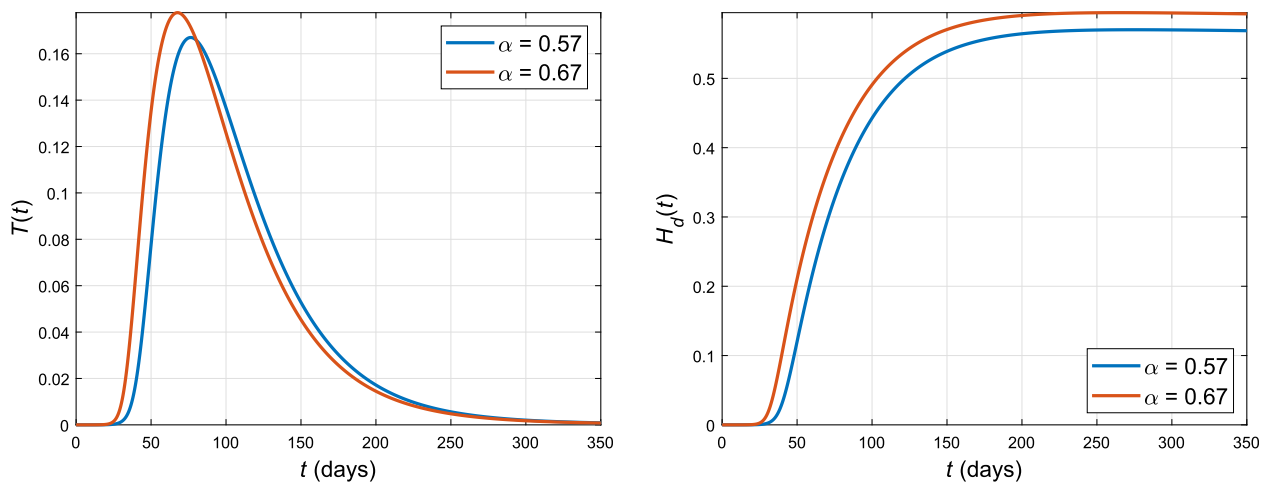**Fig. 10.** The state variables $R(t)$ and $I_r(t)$ for different values of α.

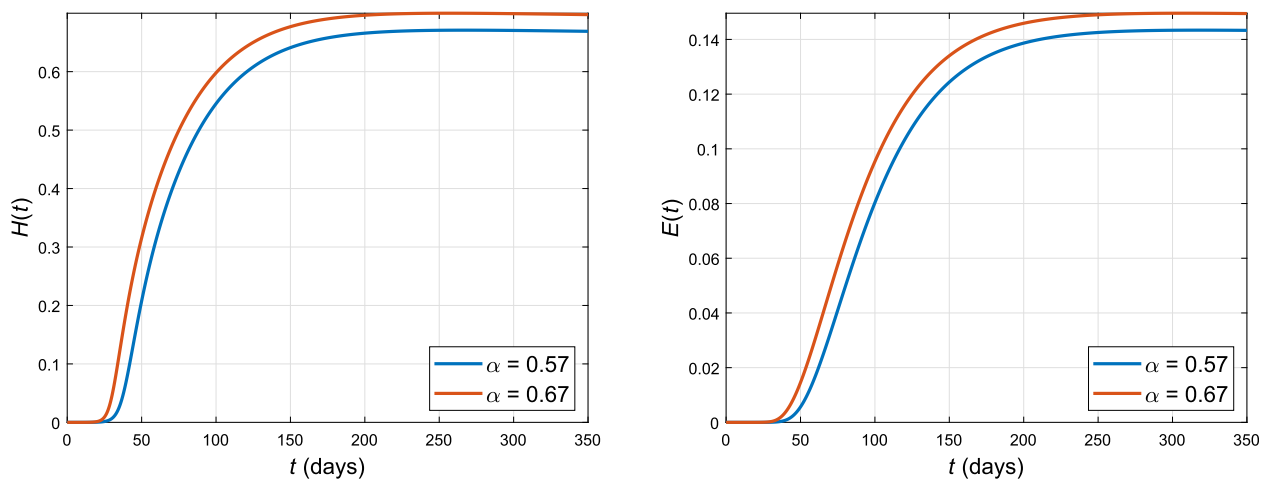**Fig. 11.** The state variables $T(t)$ and $H_d(t)$ for different values of α.

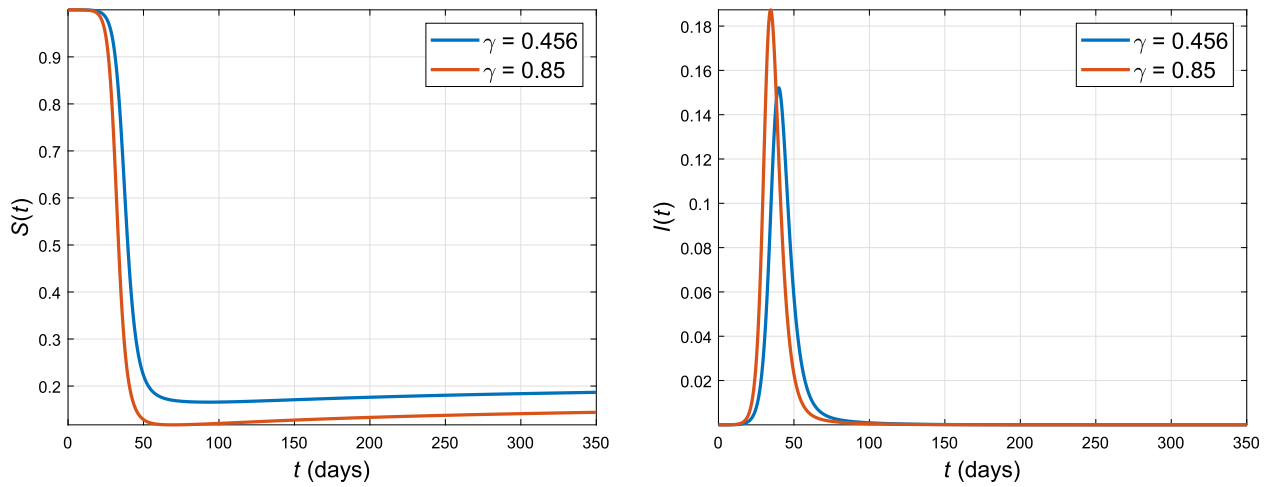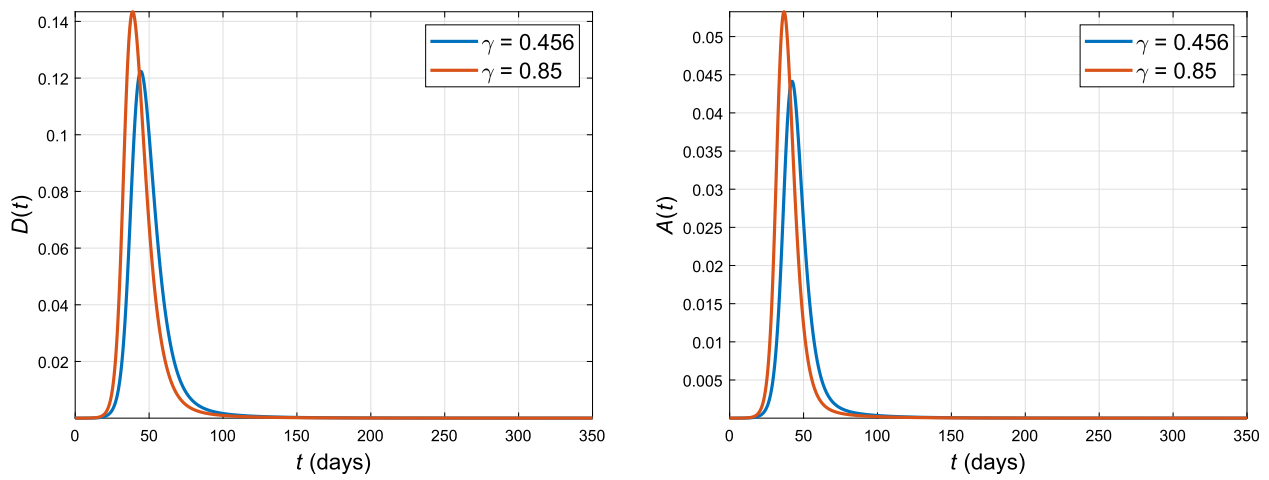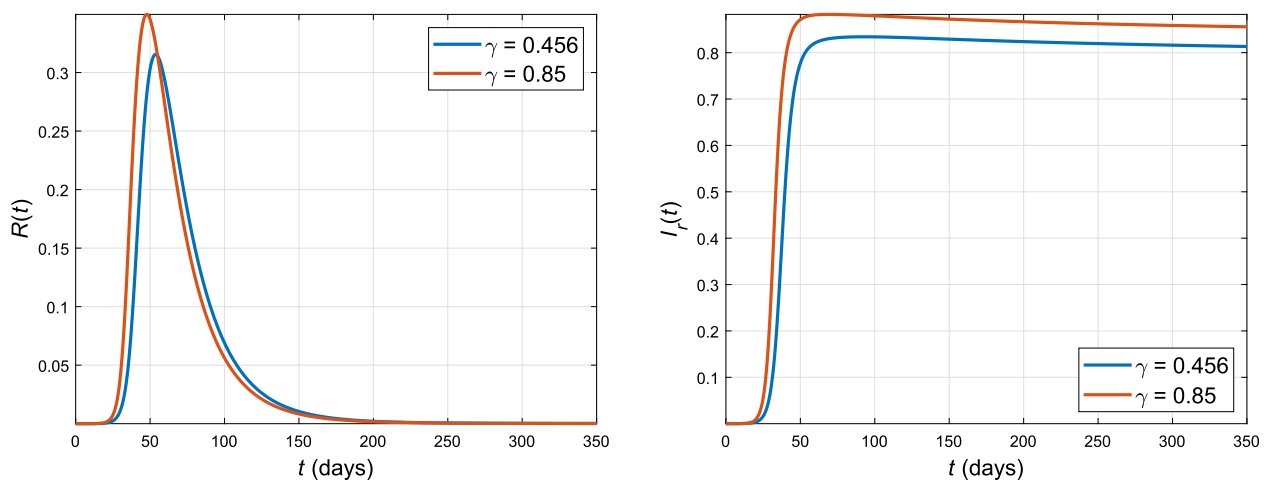**Fig. 12.** The state variables $H(t)$ and $E(t)$ for different values of α.

Fig. 13. The state variables $S(t)$ and $I(t)$ for different values of γ.

Fig. 14. The state variables $D(t)$ and $A(t)$ for different values of γ.

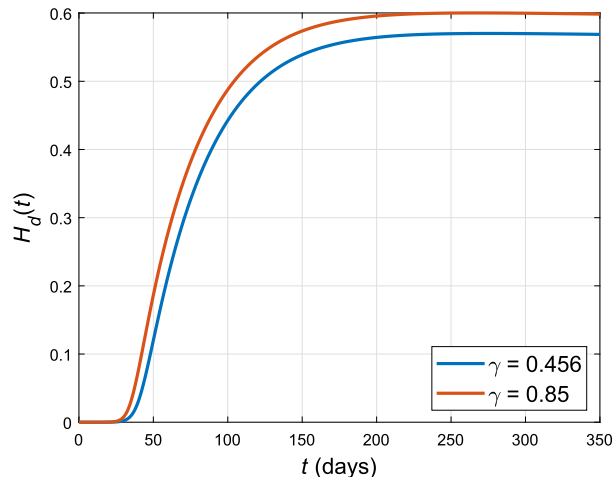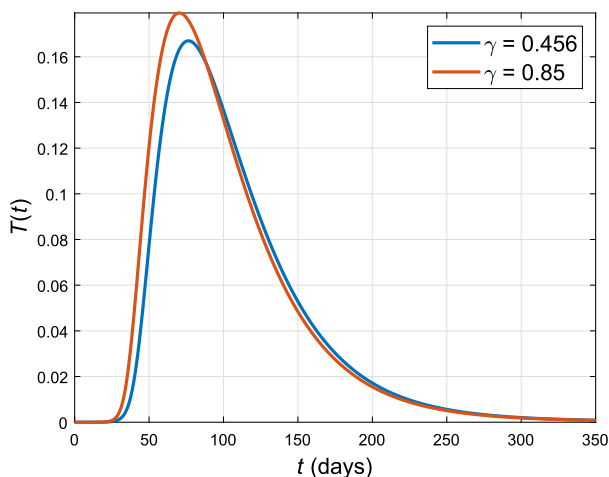**Fig. 15.** The state variables $R(t)$ and $I_r(t)$ for different values of γ.

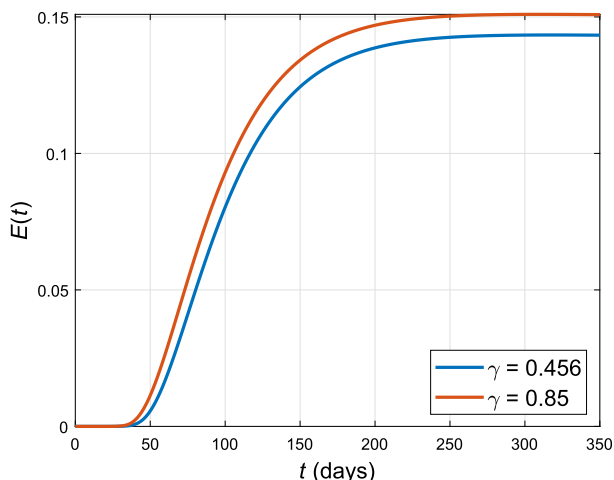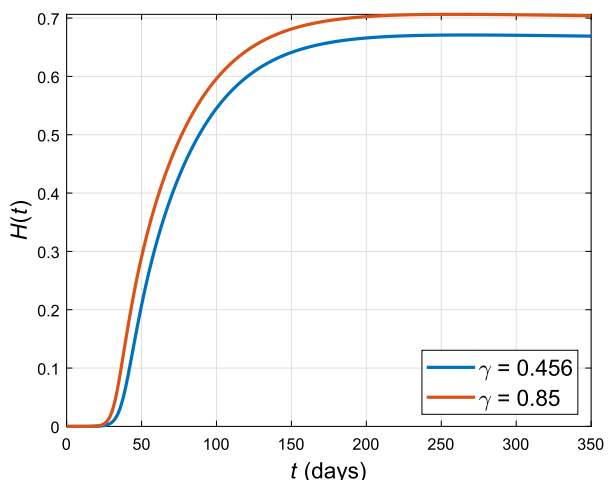**Fig. 16.** The state variables $T(t)$ and $H_d(t)$ for different values of γ.

Fig. 17. The state variables $H(t)$ and $E(t)$ for different values of γ.

CRediT author statement

Dumitru Baleanu: Conceptualization, Supervision. **Sadia Arshad:** Writing – original draft, Methodology. **Amin Jajarmi:** Validation, Writing – review & editing. **Waseem Shokat:** Writing – original draft, Software. **Fahimeh Akhavan Ghassabzade:** Investigation, Writing – review & editing. **Mubashara Wali:** Software, Investigation.

Compliance with Ethics Requirements

This article does not contain any studies with human or animal subjects.

Declaration of Competing Interest

The authors declare that they have no known competing financial interests or personal relationships that could have appeared to influence the work reported in this paper.

References

[1] Zhao TH, Castillo O, Jahanshahi H, Yusuf A, Alassafi MO, Alsaadi FE, Chu Y-M. A fuzzy-based strategy to suppress the novel coronavirus (2019-NCOV) massive outbreak. Appl Computat Math 2021;20(1):160–76.

[2] Hassan TS, Elabbasy EM, Matouk AE, Ramadan RA, Abdulrahman AT, Odinaev I. Routh-Hurwitz stability and quasiperiodic attractors in a fractional-order model for awareness programs: applications to COVID-19 pandemic. Discr Dynam Nat Soc 2022;2022:1939260.

[3] Baleanu D, Hassan Abadi M, Jajarmi A, Zarghami Vahid K, Nieto JJ. A new comparative study on the general fractional model of COVID-19 with isolation and quarantine effects. Alexandria Eng J 2022;61(6):4779–91.

[4] Nazeer M, Hussain F, Ijaz Khan M, Asad-ur-Rehman ER, ElZahar Y-M, Chu MY Malik. Theoretical study of MHD electro-osmotically flow of third-grade fluid in micro channel. Appl Math Comput 2022;420:126868.

[5] Chu Y-M, Shankaralingappa BM, Gireesha BJ, Alzahrani F, Ijaz Khan M, Khan SU. Combined impact of Cattaneo-Christov double diffusion and radiative heat flux on bio-convective flow of Maxwell liquid configured by a stretched nano-material surface. Appl Math Comput 2022;419:126883.

[6] Zhao T-H, Ijaz Khan M, Chu Y-M. Artificial neural networking (ANN) analysis for heat and entropy generation in flow of non-Newtonian fluid between two rotating disks. Math Methods Appl Sci 2021. doi: https://doi.org/10.1002/mma.7310.

[7] Chu Y-M, Bashir S, Ramzan M, Malik MY. Model-based comparative study of magnetohydrodynamics unsteady hybrid nanofluid flow between two infinite parallel plates with particle shape effects. Math Methods Appl Sci 2022. doi: https://doi.org/10.1002/mma.8234.

[8] Z.-Y. He, A. Abbes, H. Jahanshahi, N.D. Alotaibi, Y. Wang, Fractional order discrete-time SIR epidemic model with vaccination: Chaos and complexity, Mathematics, 10(2)(2022) 165.

[9] Ahmed N, Shahid N, Iqbal Z, Jawaz M, Rafiq M, Shaikh T, Ahmad MO. Numerical modeling of SEIQV epidemic model with saturated incidence rate. J Appl Environ Biol Sci 2018;8(4):67–82.

[10] Giordano G, Blanchini F, Bruno R, Colaneri P, Di Filippo A, Di Matteo A, Colaneri M. Modelling the COVID-19 epidemic and implementation of population-wide interventions in Italy. Nat Med 2020;26:855–60.

[11] Matouk AE. Advanced Applications of Fractional Differential Operators to Science and Technology. IGI Global 2020. doi: https://doi.org/10.4018/978-1-7998-3122-8.

[12] Almatroud AO, Matouk AE, Mohammed WW, Iqbal N, Alshammari S. Self-excited and hidden chaotic attractors in Matouk's hyperchaotic systems. Discr Dynam Nat Soc 2022;2022:6458027.

[13] Jajarmi A, Baleanu D, Zarghami Vahid K, Mohammadi Pirouz H, Asad JH. A new and general fractional Lagrangian approach: a capacitor microphone case study. Results in Phys 2021;31:104950.

[14] Karthikeyan K, Karthikeyan P, Baskonus HM, Venkatachalam K, Chu Y-M. Almost sectorial operators on Ψ-Hilfer derivative fractional impulsive integro-differential equations. Math Methods Appl Sci 2021. doi: https://doi.org/10.1002/mma.7954.

[15] Iqbal MA, Wang Y, Miah MM, Osman MS. Study on Date-Jimbo-Kashiwara-Miwa equation with conformable derivative dependent on time parameter to find the exact dynamic wave solutions. Fract Fract 2022;6(1):4.

[16] Wang F, Khan MN, Ahmad I, Ahmad H, Abu-Zinadah H, Chu Y-M. Numerical solution of traveling waves in chemical kinetics: Time fractional fishers equations. Fractals 2022;30(2):2240051.

[17] Momani S, Maayah B, Arqub OA. The reproducing kernel algorithm for numerical solution of Van der Pol damping model in view of the Atangana-Baleanu fractional approach. Fractals 2020;28(08):2040010.

[18] Jin F, Qian Z-S, Chu Y-M, ur Rahman M. On nonlinear evolution model for drinking behavior under Caputo-Fabrizio derivative. J Appl Anal Comput 2022. https://doi.org/10.11948/20210357.

[19] Momani S, Arqub OA, Maayah B. Piecewise optimal fractional reproducing kernel solution and convergence analysis for the Atangana–Baleanu–Caputo model of the Lienard's equation. Fractals 2020;28(08):2040007.

[20] Djennadi S, Shawagfeh N, Arqub OA. A fractional Tikhonov regularization method for an inverse backward and source problems in the time-space fractional diffusion equations. Chaos, Solitons & Fractals 2021;150:111127.

[21] Djennadi S, Shawagfeh N, Arqub OA. A numerical algorithm in reproducing kernel-based approach for solving the inverse source problem of the time–space fractional diffusion equation. Partial Diff Eqs Appl Math 2021;4:100164.

[22] Matouk AE, Khan I. Complex dynamics and control of a novel physical model using nonlocal fractional differential operator with singular kernel. J Adv Res 2020;24:463–74.

[23] Matouk AE. Chaos and bifurcations in a discretized fractional model of quasi-periodic plasma perturbations. Int J Nonlinear Sci Numer Simul 2021. doi: https://doi.org/10.1515/ijnsns-2020-0101.

[24] Kumar S, Matouk AE, Chaudhary H, Kant S. Control and synchronization of fractional-order chaotic satellite systems using feedback and adaptive control techniques. Int J Adapt Control Signal Process 2021;35(4):484–97.

[25] Matouk AE. Chaotic attractors that exist only in fractional-order case. J Adv Res 2022. doi: https://doi.org/10.1016/j.jare.2022.03.008.

[26] Matouk AE. A novel fractional-order system: Chaos, hyperchaos and applications to linear control. J Appl Comput Mech 2021;7(2):701–14.

[27] Abdurahman F, Fante KA, Aliy M. Malaria parasite detection in thick blood smear microscopic images using modified YOLOV3 and YOLOV4 models. BMC Bioinform 2021;22(2021):112.

[28] Altaf Khan M, Ullah Saif, Farhan M. The dynamics of Zika virus with Caputo fractional derivative. AIMS Math 2019;4(1):134–46.

[29] Jajarmi A, Arshad S, Baleanu D. A new fractional modelling and control strategy for the outbreak of dengue fever. Physica A 2019;535:122524.

[30] Ministero della Salute (Italian Ministry of Health), 5 April 2020, http://www.salute.gov.it/imgs/C_{17}-notizie-4403-0-fle.pdf.

[31] Podlubny I. Fractional Differential Equations: An Introduction to Fractional Derivatives, Fractional Differential Equations, to Methods of Their Solution and Some of Their Applications. New York: Academic Press; 1999.

[32] Baleanu D, Diethelm K, Scalas E, Trujillo JJ. Fractional Calculus: Models and Numerical Methods. Singapore: World Scientific; 2012.

[33] Diethelm K. A fractional calculus based model for the simulation of an outbreak of dengue fever. Nonlinear Dyn. 2013;71:613–9.

[34] Shah K, Bushnaq S. Numerical treatment of fractional endemic disease model via Laplace Adomian decomposition method. J Sci Arts 2017;2(39):257–68.

[35] Bonyah E, Khan MA, Okosun KO, Gómez-Aguilar JF. Modelling the effects of heavy alcohol consumption on the transmission dynamics of gonorrhea with optimal control. Math Biosci 2019;309:1–11.

[36] Khan MA, Ali K, Bonyah E, Okosun O, Islam S, Khan A. Mathematical modeling and stability analysis of Pine Wilt Disease with optimal control. Scient Rep 2017;7:3115.